Examination and Evaluation of Safe End From Nozzle N6B on Nine Mile Point Reactor

DC-65

5 March, 1970

Prepared for: Division of Compliance
United States Atomic Energy Commission

AEC Contract No. AT(11-1)-1658

Parameter No. DC-65 Subcontract No. 5

Prepared by: R. W. Staehle
Columbus, Ohio

Prepared through: Parameter, Inc.
Consulting Engineers
Elm Grove, Wisconsin

Enclosure 1

TABLE OF CONTENTS

	Page
1.0 Summary and Conclusions	1
2.0 Background and Introduction	2
3.0 Experimental and Specimens	2
4.0 Results	4
4.1 Optical and Scanning Metallography	4
4.1.1 General Examination of the Inside Surface	4
4.1.2 Cross Sectional Examination of Cracks Starting at Inside Surface	4
4.1.3 Cross Sectional Examination of Cracks Starting at Outside Surface	5
4.1.4 Examination of the Crack Face	5
4.1.5 Examination of the Field Weld and Weld Affected Zone	6
4.2 Electron Probe Results	7
4.2.1 Traces Across Crack Cross Section	7
4.2.2 Analysis of Oxide Found in Cross Sectional Examination	8
4.2.3 Analysis of Oxide on the Crack Surface	8
5.0 Discussion	10
5.1 Mode of Cracking from Inside Surface	11
5.2 Causative Elements	11
5.3 Sequence of Events	14
5.4 Significance of Transgranular Cracking	16
5.5 Significance of Intergranular Penetrations on Material Not Furnace Sensitized	16
5.6 Confidence Level for Safe Ends If Not Repaired	16

Table of Contents (Continued)

Page

5.7 Implications for Repair Procedure 17

5.8 Mechanistic Processes 17

6.0 Acknowledgements. 17

7.0 References. 18

List of Figures

1. Schematic diagram showing safe end configuration.
2. Schematic description of radiographic indications from safe end showing location of cracks. The 12:00 position was the top of the tube. Radiographs were taken through the double thickness of the tube before specimens were removed. Location of the AEC specimen is noted. Approximate location of leaks noted.
3. Schematic location of cuts made in the core spray line for removing the AEC-GE specimen. Cut numbers refer to same numbers of figure 1.
4. Schematic arrangement showing orientation and description of AEC specimen. (a) Orientation of specimen with respect to tube and coordinate axes. (b) Letter designations describing specimens taken from AEC specimen, together with coordinate axes. (c) Optical macrographs showing views of inside surface, edges, and end of AEC specimen. Only that portion shown in the -x direction from the field weld.
5. Optical macrograph showing view of inside surface of the AEC specimen. Coordinates relate to figure 4. Circled region shows site where scanning electron micrograph obtained (figure 6).
6. Scanning electron micrograph from inside surface of AEC specimen. Note site of micrograph in figure 5.
7. Optical micrograph of crack starting at inside surface and extending in the +z direction. Specimen taken from specimen B. Face being examined is in the x-z plane. Left figure is initial portion of crack and right figure is bottom. The bottom of the left figure and top of right are exactly contiguous.
8. Optical micrograph of crack starting at inside surface and extending in the +z direction. Specimen taken from specimen B. Face being examined is in the x-z plane. Left figure is initial portion of crack and right figure is bottom. The bottom of the left figure and top of right are exactly contiguous.

9. Optical micrograph of crack starting at inside surface and extending in the +z direction. Specimen taken from specimen E. Face being examined is in the x-z plane. Left figure is initial portion of crack and right figure is bottom. The bottom of the left figure and top of right are exactly contiguous.

10. Schematic arrangement showing location of specimens taken from outside surface of specimen B. Surface viewed is in the x-z plane.

11. Photomicrographs of cracks on outside surface of specimen B. Cracks are propagating in the -z direction. Surface viewed in the x-z plane.

12. View of face of crack. Crack face is in the y-z plane. Specimen broken apart for viewing. (a) Color print (b) Schematic diagram showing various regions of crack. Distances from inside surfaces noted locate sites where scanning micrographs taken. Specimen broken open to show surface of stress corrosion crack. Shiny bright region results from this breaking process.

13. Scanning electron micrographs of stress corrosion crack surface corresponding to 0 mm position noted in figure 12.

14. Scanning electron micrographs of stress corrosion crack surface corresponding to 1 mm position noted in figure 12.

15. Scanning electron micrographs of stress corrosion crack surface corresponding to 3 mm position noted in figure 12.

16. Scanning electron micrographs of stress corrosion crack surface corresponding to 5-1/2 mm position noted in figure 12.

17. Scanning electron micrographs of stress corrosion crack surface corresponding to 8 mm position noted in figure 12.

18. Optical micrograph from specimen H along inside surface along d_2-d_3. Plane viewed is x-z.

19. Optical micrograph from specimen H along the outside surface along d_2-d_3. Plane viewed is x-z.

20. Optical micrograph from specimen K showing inside surface along e_2-e_3. Plane viewed is x-z.

21. Optical micrographs from specimen K showing outside surface. Penetrations are extending in the -z direction from the surface. The plane viewed here is along the e_2-f_2 line.

22. (a) Schematic location showing where microprobe trace across crack was performed. (b) Photographs showing where traces performed. (c)-(d) Results from separate determination at different sites along crack.

23. Typical oxide in crack showing where the x-ray spectrum was analyzed. This is not the region examined but the oxide is typical.

24. Intensity of x-ray emissions from spectral scan of one piece of oxide in crack by microprobe. Spectral regions where primary peaks should have occurred for particularly sought elements are noted with asterisk.

25. Montage showing scanning micrograph from face of stress corrosion crack. Special notations locate regions where microprobe determinations were made. The location of each micrograph is the same as that in figure 12. Most of the scanning micrographs are from the series shown in figures 13-17. For reference the Cr/Fe ratio of scale-free type 304 stainless steel is 0.4. These ratios are from direct scale readings and are not corrected.

26. Schematic relationship showing possible pattern of interaction of stress, sensitization, dissolved oxygen, temperature at pH in the stress corrosion cracking of sensitized stainless steels.

1.0 Summary and Conclusions

A safe end from a core spray line was removed and examined from the Nine Mile Point Reactor; this was from nozzle N6B at the west core spray safe end. This specimen was examined because small leaks were observed during a reactor shutdown. A portion of this specimen was examined at Battelle Northwest Laboratories at the request of the AEC; the remainder was examined by General Electric personnel. The BNWL-AEC investigation was performed according to a procedure outlined by R. W. Staehle and W. J. Collins. The investigation at BNWL was supervised by L. A. Hartcorn. This report describes and analyzes only the examination at BNWL.

Important conclusions from the examination at BNWL are as follows:

1. The failure was most likely caused by stress corrosion cracking of heavily sensitized stainless steel as opposed to the possibility of fatigue or overload.
2. There is a high probability that the failure initiated and propagated while the reactor was at power.
3. The cracking was intergranular and started from the inside surface. A small amount of transgranular cracking started from the outside surface, but the intergranular cracking caused the observed leaks.
4. The primary causative elements in this failure are most reasonably heavy sensitization, high stress, and dissolved oxygen. Minor causative elements may be slightly lowered pH (relative to PWR's) and elevated temperature (relative to room temperature). If any one of the primary causative elements had been negligible, cracking would probably not have occurred. The minimum critical combinations of individual values of the primary causative elements are not clear. The form of stress corrosion cracking described herein has been observed to occur at room temperature (Oyster Creek).

2.0 Background and Introduction

This report describes the observations and their analysis made on a specimen removed from nozzle N6B at the west core spray nozzle safe end in the Nine Mile Point Reactor. This reactor is operated by Niagara Mohawk Power Corp.

The specimen described in this report was removed during the weekend of 14-15 March 1970. It was carried by W. J. Collins of AEC to Battelle Northwest Laboratories in Richland Washington. Significant portions of this examination were completed by 24 March, 1970.

The specimen was removed from the safe end of the core spray nozzle at a point outboard of the weld between the carbon steel and the safe end.

Removal of this particular specimen was based on a leak observed while the reactor was shut down. The leak took the form of a fine spray and penetrated the pipe at two points.

This report describes specifically the operations involved in removing the specimen, the procedures and results of examination, and an analysis of the possible causes of failure.

3.0 Experimental and Specimens

The region from which the specimen was removed is shown in figure 1. The region of cracking was determined from radiography performed before the specimen was removed. The arrangement of cracks as determined in radiography is shown schematically in figure 2. This radiograph was taken by GE personnel and the determination was made through a double thickness of metal (i.e. through both walls).

The specimen was removed from its installed location using a power hacksaw. No coolant was used during the operation. A schematic arrangement of the location from which the specimen was removed together with the cuts is shown in figure 3. The first cut was made approximately at position #1.

When this cut was completed, the portion of the pipe connected to the vertical riser shifted to the left about 3/4" relative to the portion of the pipe connected to the vessel. This resulted from the locked in deformation (cold spring) in the piping; this was thus relieved where the cut was made. Following the first cut a second one was made at position #2. This cut formed the outer boundary of the specimen. Following this cut a shielding plug was inserted to prevent radiation streaming. Special care was taken during this operation to avoid damaging the inside surface mechanically or introducing chemical contamination. The final cut was made at position #3 and this formed the other boundary of the specimen. The specimen as cut contained both material from the furnace sensitized safe end as well as non-sensitized pipe. The portion of this pipe next to the weld can be presumed to be slightly sensitized.

The entire "specimen" for both the AEC and GE constituted the region between cuts #2 and #3 of figure 3. The portion examined at Battelle Northwest on behalf of the AEC was the length of the specimen tube and one inch wide; it was taken approximately from the site shown on the radiographic layout of figure 2 and shown also in figure 4. This location was between the 10:45 and 11:00 positions with the 12:00 being straight up. This particular location was selected to give GE the opportunity to examine both leaks.

For convenience herein the specimen described in this report will be called the "AEC specimen" and the remainder will be called the "GE specimen." The entire specimen taken between the cuts #2 and #3 will be called the "AEC-GE specimen."

The AEC specimen was cut by Niagara Mohawk personnel using a dry milling procedure. (i.e. no coolant was used). This cutting operation, as well as the one involving taking the entire specimen, was monitored by Staehle and Collins. Special care was taken to avoid spurious contamination. The AEC specimen was taken by Collins to BNWL on 15 March, 1970.

The GE-AEC specimen is shown in figure 4 with respect to orientations and specimen designations. X-y-z coordinates are applied for convenience in describing the specimen. In addition to these directions a series of letter designations (a_1-b_2 etc.) outline specific interfaces.

The AEC specimen was cut by manual hacksaw into the specimens shown in figure 4b. Figure 4c shows the part of the AEC specimen before it was cut into smaller specimens for subsequent evaluation.

The specimen was examined by BNL people using the following techniques: optical metallography, scanning electron metallography (SEM), electron microprobe analysis. No unusual or novel techniques were employed. These techniques were applied to this analysis in ways that are relatively straight forward in failure analysis.

4.0 Results

This section describes the results from examinations using optical and electron metallography and micro-probe analysis.

4.1 Optical and Scanning Metallography

4.1.1 General Examination of the Inside Surface

Figure 5 shows an inside view of the AEC specimen surface where the cracking was most extensive. This cracking was most extensive next to cut number 3, i.e. the end of the specimen toward the reactor vessel.

Figure 6 is a scanning electron micrograph from the region circled in figure 5. This shows the inside surface of the pipe and looks into the crack in the +z direction. The cracking is clearly intergranular. There appears to be little evidence of any significant plastic deformation. A further significant observations here is that there is no pattern of intergranular penetration on the surface. This suggests that the cracking process is not a stress assisted intergranular corrosion but is a type of stress corrosion cracking.

4.1.2 Cross Sectional Examination of Cracks Starting at Inside Surface

Figures 7 and 8 are optical micrographs from specimen B on the a_2-b_2 face looking in the +y direction. The cracks start from the inside surface and progress in the +z direction. On these figures it should be particularly noted that there is little evidence of significant plastic behavior of the material. There are no strain markings nor do the grains at the fracture edge have a "taffy-like" appearance indicative of gross local plastic deformation.

This observation is significant in the latter discussion where the differences between stress corrosion cracking and purely mechanical failures are discussed. The former usually exhibits little local deformation associated with the crack.

Figure 9 is an optical micrograph showing a crack from specimen E along the b_2-c_3 face and looking in the +y direction. This cracking mode is again intergranular but the extent drops off with the distance away (+x direction) from a_1-a_4 interface. This suggests that residual stresses from the weld and also the adjacent thickness discontinuity (See Fig. 1) interacted with the moment in the pipe due to differential expansion of the vessel and vertical pipe. This moment was presumably constant over the safe end. This interaction suggests that the observed cracking is strongly stress dependant. It further suggests that the crack may have initiated and propagated only when the reactor was at power.

4.1.3 Cross Sectional Examination of Cracks Starting At Outside Surface

The outside surface of the AEC specimen was also examined metallographically. Figure 10 shows schematically where a specific set of specimens was taken from specimen B. These specimens were taken from the a_2-b_2 face of specimen B and looking in the +y direction. The capital letters (A,B,C ...) indicate approximate locations where micrographs were taken. These micrographs are shown in figure 11 and have letter designations corresponding to those of figure 10. Figure 11 shows that transgranular cracks had initiated from the outside surface. Some of the specimens show extensive evidence of strain markings near the surface. These should be compared with the edge of the crack in figures 8 and 9 where no such strain markings are evident. This comparison is again significant with respect to establishing whether the intergranular cracking from the inside surface was due to stress corrosion or to a purely mechanical type of failure. The strain markings of figure 11 are no doubt the result of rough handling of the piping during construction. This amount of cold work, in itself, at this location is probably not significant. The point to be made here is simply that the evidence of strain markings on the surface is not associated with the intergranular cracks.

Another factor of significance is the relatively limited extent of these cracks into the metal. Since relatively high stresses are known to be required for the intergranular cracks and since the chloride induced transgranular cracks propagate easily at 20-50% of the yield, it would seem that the transgranular cracks would have progressed further if the chloride were present at the site of cracking over the entire duration of the plant operation. While there are obvious alternatives to this interpretation (i.e. lack of moisture, too low a chloride concentration), this limited extent of cracking will be discussed later with respect to fixing the time of cracking.

4.1.4 Examination of the Crack Face

The surfaces of the cracks were examined optically and a color photograph of the cracked surface is shown in figure 12a. The cracked surface appears to have three zones. The first (next to the inside surface) is generally dark brown; the next is a dull gray; and the third (next to crack root) is a bright gray. Beyond this the shiny bright region is the result of breaking the specimen open to expose the surface.

These different regions on the crack face were examined using the scanning electron microscope. A series of pictures at various magnifications was taken at each of these discrete regions. A schematic figure showing these regions is given in figure 12b. The scanning electron micrographs are shown in figures 13-17. These figures are designated as 0 mm, 1 mm, 3 mm, 5-1/2 mm, and 8 mm - these being the respective distances away from the inner surface in the +z direction. The plane of the crack surface is approximately parallel to the y-z plane.

The micrographs of figures 13-17 show clearly that the crack is intergranular and that very little gross plastic deformation occurred.

Of particular interest, especially at the higher mangifications is the morphology of the corrosion product. The corrosion product on the 5-1/2 mm point (figure 16) has a shape often found on surface exposed to high temperature water at high pH[1]. These shapes are typical of those formed by precipitation from the solution. The precipitates at the 3 mm site (figure 15) appear to have some structure but to be less well formed. At 1 mm (figure 14) the precipitates seem to have little structure at all. At the 0 mm (figure 13) site, just inside the inside surface of the specimen, the precipitates

form an altogether different shape. The essential features of this shape is a spherical "pebble" with "needles" enumating from the surface. The micrograph of the intentionally broken region at 8 mm (figure 15) shows the expected ductile behavior.

4.1.5 Examination of the Field Weld and Weld Affected Zone

The region of the field weld was examined to provide a comparison between the behavior of furnace sensitized material and the weld sensitized material.

Figure 18 shows a weld defect on the ID surface from specimen H looking in the y direction on the c_2-d_2 face. The apparent defect runs along the d_2-d_3 line. There is no clear evidence for this defect being caused by SCC but it may have been. The general appearance suggests that it may be due to a weld defect.

Figure 19 shows the weld region on the outside diameter of specimen H along the line d_2-d_3. No gross attack is evident here.

Figure 20 shows the inside diameter from specimen K along the line e_2-e_3. Some intergranular penetration is evident here although it appears to have extended inward only a relatively small fraction of a grain diameter.

Figure 21 shows a set of micrographs from the outside surface of specimen K along the interface e_2-f_2. A small amount of intergranular penetration is noted in all cases. These pictures were taken to ascertain the behavior of the weld sensitized region; however, it is not possible to determine whether these intergranular penetrations are related to pickling of the tubing prior to installation or are related to a stress corrosion process which occurred during the operation of the reactor.

4.2 Electron Probe Results

Three regions were examined to determine local chemical composition using the microprobe. Traces were made across the cross section of cracks; individual oxide particles found in cross sections were examined; and the composition of the precipitates on the crack faces was determined. Depending on the site, various chemical elements were sought.

4.2.1 Traces Across Crack Cross Section

Figure 22a is a schematic diagram showing the region examined by a microprobe scan; figure 22b shows scanning micrographs of the regions examined; figure 22c and d are results from scans across the crack. These scans were conducted step-wise across the cracks. The concentrations of these elements were calculated using an analyzed Type 316* stainless steel standard. Steps were taken at 0.5 micron intervals. These scans were conducted on the a_1-b_1 surface of specimen A. The zero point of the coordinates was taken as the center of the crack. The trace was taken to be approximately perpendicular to the plane of the crack face. No particularly unusual distribution of iron, chromium, or nickel was noted. The composition of all the elements naturally decreased in the vicinity of the crack. The slight humps and irregularities are associated with grayish precipitates.

4.2.2 Analysis of Oxide Found in Cross Sectional Examination

The oxide material in a crack similar to the one shown in figure 23 was analyzed for the entire spectrum of elements starting with the element magnesium. Only elements Fe, Cr, Ni, Mn and a trace of Si and Mn were detected. Special attention was directed toward finding elements Cu, F, Cl, Br, Pb, S, As, but none was found in significant quantities above the minimum sensitivity of 0.03 to 0.1 weight percent. There appears to be a slight indication of copper enrichment. The enrichment of copper on iron base surfaces is common because high purity water is often exposed to heat exchangers constructed

---

* This material was used because the iron, chromium, and nickel had been chemically analyzed. Thus the x-ray emissions from the subject experiments could be compared with the peak heights from the 316 and the appropriate experimental corrections made. The Type 316 was used because of the press of time and because its use is considered to involve virtually no error.

of copper base alloys. Figure 24 shows the result of the scan of the spectrum. On figure 24 the various spectral peaks are designated for the respective alloy elements which were found. Also the locations of primary peaks for other elements, sought but not found, are noted.

4.2.3 Analysis of Oxide on the Crack Surface

Figures 13-17 showed distributions and morphologies of precipitates on the crack surface. The chemical composition of these precipitates was determined approximately using the microprobe. Figure 25 shows the complete set of results including the site from which the analyses were taken and the Cr to Fe ratio as determined directly from the x-ray peaks for the two elements. In addition, for comparison, the morphology and chemistry of surface scale is shown in figure 25. There are three very important observations here:

1. The Cr/Fe ratios are generally higher than that in the alloy. The theoretical ratio in the alloy is Cr:Fe = 18:74 = 0.24. However, the uncorrected ratio from x-ray emission from examining a clean surface is 0.4. Thus, the ratios in figure 25 should be compared with the latter number.

2. The Cr/Fe ratio at the crack mouth is very high.
3. There are wide local ranges as noted at the 3 mm position.

The basis for these enrichments in chromium appear to be related to the relative solubility products of the iron hydroxides and chromium hydroxide. The latter are less soluble and therefore would tend to precipitate earlier. The enrichment at the crack mouth is probably relavent to a change in pH

thereat. Work on chemistries in restricted geometries has shown that inside cracks of iron base alloys the pH at room temperature lies in a range of about pH = 3.0. Presumably the basis for the very great enrichment of Cr at the 0 mm position is related to the great driving force for precipitation when the pH changes from that inside the crack (low pH) to that in the bulk environment (neutral pH).

The wide range of Cr/Fe ratios at the 3 mm position suggests that the crystals formed at different times when the solution contained widely varying ratios of Fe and Cr soluble ions. For example, the Cr/Fe = 0.8 value was from a generally broad area which certainly includes some of the substrate. Most of the dissolution contributing to the enriched chromium may have come from the dissolution of the carbides which are rich in chromium. The iron rich crystals may have come at a time when the chromium free zone was dissolving at the tip of the propagating crack.

The octahedral morphology of the crystals at the 5-1/2 mm position of figure 25 has been observed before by Kabele and Daniel[1] who examined the corrosion products on stainless steel surfaces in static autoclaves. This octahedral morphology is that usuallly preferred by magnetite.

The difference in Cr/Fe ratio of the "pebbles" and "needles" at the 0 mm position suggest again that the composition of the solution inside the crack changes with time. Thus, it is reasonable that the first precipitate to form, i.e. the inside or pebble part, is higher in chromium because of its lower solubility product; the needles are still high in chromium but have a relatively lower Cr/Fe ratio.

The relatively high Cr/Fe ratio found in the surface scale of figure 25 suggests that the dissolving alloy precipitates so that the chromium is enriched according to the previous comment concerning the effect of pH on solubility products.

5.0 Discussion

The essential technical objectives for this investigation were to supply the kind of information necessary to answer or assess the following questions:

1. Was the cracking mode related to stress corrosion cracking, high strain range low cycle fatigue, or mechanical overload?

2. If the failure mode is stress corrosion cracking, what were the causative elements and their relative importance (temperature, degree of sensitization, oxygen, stress)?

3. With respect to a possible stress corrosion failure what is the most likely sequence of events?

4. What is the significance of the transgranular cracking observed on the outside surface?

5. What is the significance of the intergranular penetrations in the region next to the weld opposite the safe end?

6. To what degree of confidence is information available that would permit leaving some of the safe ends in the vessel without repair?

7. To what degree of confidence can a repair procedure be specified based on the information herein?

The following discussion is addressed to these questions. In addition, there is a brief discussion of the mechanistic processes involved in the stress corrosion cracking of sensitized material.

5.1 Mode of Cracking from Inside Surface

Figures 5-9 and 13-17 suggest, without much question, that the failure mode was stress corrosion cracking. There is very little evidence for local plastic deformation which would support a view of fatigue or overload failures. If either of these latter two modes were operating, the grains, for example, in figures 7-9 would have a taffy-like pulling apart appearance. Also, the etch would have shown the kind strain makings which were observed near the surface of figure 11.

There is no evidence that this failure is simply an intergranular corrosion phenomenon which was accelerated by stress. The SEM micrograph of figure 6 shows no evidence of general intergranular corrosion. The only attack apparent is associated with the crack itself.*

5.2 Causative Elements

The causative elements to be considered here are:

1. Degree of sensitization
2. Applied stress
3. Dissolved oxygen
4. Other environmental contaminants
5. Temperature
6. Solution pH

There is virtually no information presently available to permit assessing very specifically the relative magnitudes and combination of the above factors which are critical with respect to causing stress corrosion cracking. Available information makes possible the following qualitative comments:

---

* This appears to be a minor distinction but it is not. For example, sensitized stainless steel would dissolve intergranularly and rapidly in boiling concentrated nitric acid; with applied stress the process would be somewhat accelerated. However, for stress corrosion cracking, no significant attack occurs unless stress is applied.

1. The sensitization required for this type of crack must be fairly extensive. The paper of Ward, Mathis and Staehle[2] shows that light sensitization is not sufficient to cause this intergranular stress corrosion cracking in fluoride contaminated solutions at room temperature. Conversely, the stainless steel fuel elements which failed intergranularly in the high power density program conducted by GE in the early 1960's (See GEAP-4400 for example) were not sensitized.

2. The stress requirement for SCC of sensitized material is not well defined but the general pattern of events suggest that it must be above the yield strength. This is generally well above the range of stress required for the transgranular cracking of stainless steel induced by chloride. For the latter case stresses as low as 10-30% of the yield strength are sufficient to cause SCC.

   The failures which occurred in the stub tubes at Oyster Creek were generally associated with the regions of highest stress; in that case the stresses were produced by welding and were shown to be very high.

   In the case of the failure described herein the magnitude of stress at the joint in question is clearly high but definitive values are not yet available. The fact that the major cracks were concentrated near the weld and the section discontinuity suggests that on the stresses causing cracking were related to a summation of the applied plus the residual welding and the discontinuity stresses.

   The stresses appear to have been highest during operation since the maximum thermal differential between the vessel and vertical portion of the core spray line occurs at this time. It should be noted that the usual argument about the inside surface in compression and outside in tension do not apply here since the neutral axis is the pipe centerline.

3. The amount of dissolved oxygen required for this intergranular SCC of sensitized material is not clear. The intergranular cracking observed to date for all causes suggest that oxygen is required but how much is not clear. The lack of a similar occurrence in PWR type systems suggests that the minimum range may be in the range of 1 ppm. The general pattern of SCC observed in various reactors together with data in the literature obtained on higher nickel alloys suggests that oxygen is certainly an accelerant.

4. In general it appears that intergranular SCC of sensitized material can occur in the absence of contaminants such as chloride, fluoride, etc. However, it also appears that these can accelerate the process as indicated by the data of Ward et al.[2] discussed earlier.

5. The critical temperature for SCC of the sensitized material is not clear. It certainly must be interrelated in some way with the other factors. However, the Oyster Creek failure suggests that cracking can occur readily at room temperature.

6. The pH of the solution is an important variable with respect to SCC and this may be part of the basis for observed differences in the behavior of BWR and PWR systems. However, this is presently a speculative matter and care should be exercised in reaching conclusions here.

The general pattern suggested by the above is that sensitivity to SCC of sensitized material can be interrelated according to the following qualitative relationship for cracking to occur:

$$[\text{stress}]^m \times [\text{degree of sensitization}]^r \times [\text{oxygen}]^p \times [\text{temperature}]^q \times [\text{contaminants}]^z \times \left[\frac{1}{\text{pH}}\right]^y > K \qquad (1)$$

i.e. cracking will occur when the product exceeds K.

One can conclude from this equation that SCC will not occur when any of these quantities is 0 (except for some obvious difficulties of interpretation associated with too low pH). Further, an approach to eliminating the SCC problem is to minimize all the factors. Graphically this SCC problem might be considered as having the dependancies shown in figure 26. This figure suggests that the two most critical parameters are stress and degree of sensitization. Below the hyperbolic lines SCC will not occur but will above; the increase of oxygen and temperature, and decreasing pH may cause these lines to shift to a broader range of cracking by going progressively from lines 3 to 2 and 1. Increasing the concentration of contaminants (like fluoride) would presumably act to move from line 3 to 1.

The exponents in equation 1 should be indicative of the dominance of their respective quantity. While this expression is only qualitative, it should serve as a reasonable basis for considering the general aspects of material-environmental control.

5.3. Sequence of Events

In assessing the sequence of events questions naturally raised include:

1. Did the failure start prior to operation?
2. Did it occur at elevated temperature?
3. Did it occur at room temperature?
4. Did it occur during heat-up or cool-down cycles?

While absolute evidence is lacking in order to be specifically definite with respect to the above questions, the evidence especially of figures 12, 13-17 suggests the following:

1. Significant propagation occurred during the last 3 to 5 cycles and each band of figure 12 corresponds to a different time when the crack was propagating.

2. Cracking probably did not occur prior to operation but this cannot be proved.

3. The excessive brown coloration of the first stage of cracking in figure 12 suggests that this region may have existed for a fairly long time. This may be the result of a large number of small increments of propagation or a simple propagation which existed very early. There is also the possibility that this propagation occurred at high temperature and the others occurred at low temperature.

4. The change in morphology of the precipitates suggests that the well formed ones at 5-1/2 mm of figure 16 were the result of cooling slowly. This implies that the last stage of cracking occurred during the last cycle and that it occurred at high temperature. This is based on the assumption that such crystals were formed while cooling down. The different shapes of precipitates at the 3-1/2 and 1 mm position suggest that at one time the well formed crystals existed but with successive thermal cycles they dissolved and reprecipitated.

5. The crack propagation appears to have involved some amount of dissolution during propagation of both the carbides and the region depleted of chromium. This helps justify the higher Cr/Fe ratios.

6. The fact that the stresses presumably are raised in the safe end considerably during hot operation provides the essential basis for an argument that crack propagation occurs while the reactor is at power.

In summary, it appears that the cracks propagated at the high temperature and did so during reactor operation.

5.4 Significance of Transgranular Cracking

The transgranular cracks observed on the outside surface as shown in figure 11 were almost certainly induced by chloride. In view of the stresses it is surprising that they have extended only such short distances. If the chloride and high stress had existed for a long time, it is likely that the transgranular cracking would have completely penetrated the wall. This lack of extent probably results from the fact that they may not have occurred until after the leak induced by the internally generated cracks. It is possible that the water deposited briefly on the outside surface was evaporated, and left (after enough evaporation) a chloride residuum. It is also possible that these cracks could have occurred earlier but the chloride concentration was not sufficient to cause significant propagation.

5.5 Significance of Intergranular Penetrations on Material Not Furnace Sensitized

Figure 21 shows intergranular penetration on the outside diameter of the pipe in the +x direction from the field weld. Their general pattern suggests that this mode of attack may have been produced during pickling. Neither possibility (pickling or in service) can be excluded by the available evidence. However, if pickling were the case, it would seem that similar penetration should have occurred on the inner surface.

5.6 Confidence Level for Safe Ends If Not Repaired

This question is not easily answered by available data. The only readily manipulable variable is stress and the question relates to a stress level below which SCC of sensitized material will not occur. It is reasonable that such a level may in fact exist and that, by taking additional specimens of equivalent geometries but at lower stresses, a reasonable estimate for a safe stress level could be obtained. However, any conclusion based on even this evidence would be questionable for the following reasons:

1. There is no clear evidence that the applied plus residual stress patterns presently existing and during reactor life can be specified with the necessary confidence.

2. The complexity of interaction suggested by equation 1 and figure 26 produce an additional degree of uncertainty that makes clear conclusions difficult.

5.7 Implications for Repair Procedure

Based on the evidence from this work it can only be said that sensitization and high stresses should be avoided. More specific recommendations are too speculative and argumentative and are not considered appropriate for this report. However, it is also appropriate to point out here that there is virtually no useful information on the mechanical properties of heavily sensitized material: i.e. fatigue, rapid crack propagation, creep rupture.

5.8 Mechanistic Processes

While this is not the appropriate place to discuss at length the mechanism for cracking, several comments are appropriate.

Sensitized stainless steel appear to crack according to an electrochemically controlled process. Oxygen serves the function of a reducible species and therefore promotes the anodic process at the crack tip. The same function would be provided by hydrogen ions if the pH is lowered. The actual propagation process appears to be related to a transient dissolution of the chromium-depleted grain boundary material; the capacity of this material to repassivate appear to be substantially reduced relative to the bulk grain containing higher chromium. Applied stress breaks the protective film; the chromium containing grains repassivate rapidly and no crack penetration occurs; the depleted region does not repassivate so rapidly and cracks propagate.

6.0 Acknowledgements

The metallographic work at BNWL was supervised by L. A. Hartcorn; microprobe analysis was performed by W. Clark; and scanning electron metallography was performed by J. L. Daniel

7.0 References

1. T. J. Kabele and J. L. Daniel, "Corrosion Product Study by Scanning Electron Microscope", BNWL-1184, November, 1969.

2. C. T. Ward, D. L. Mathis, and R. W. Staehle, Corrosion, Vol. 25., No. 9, September, (1969).

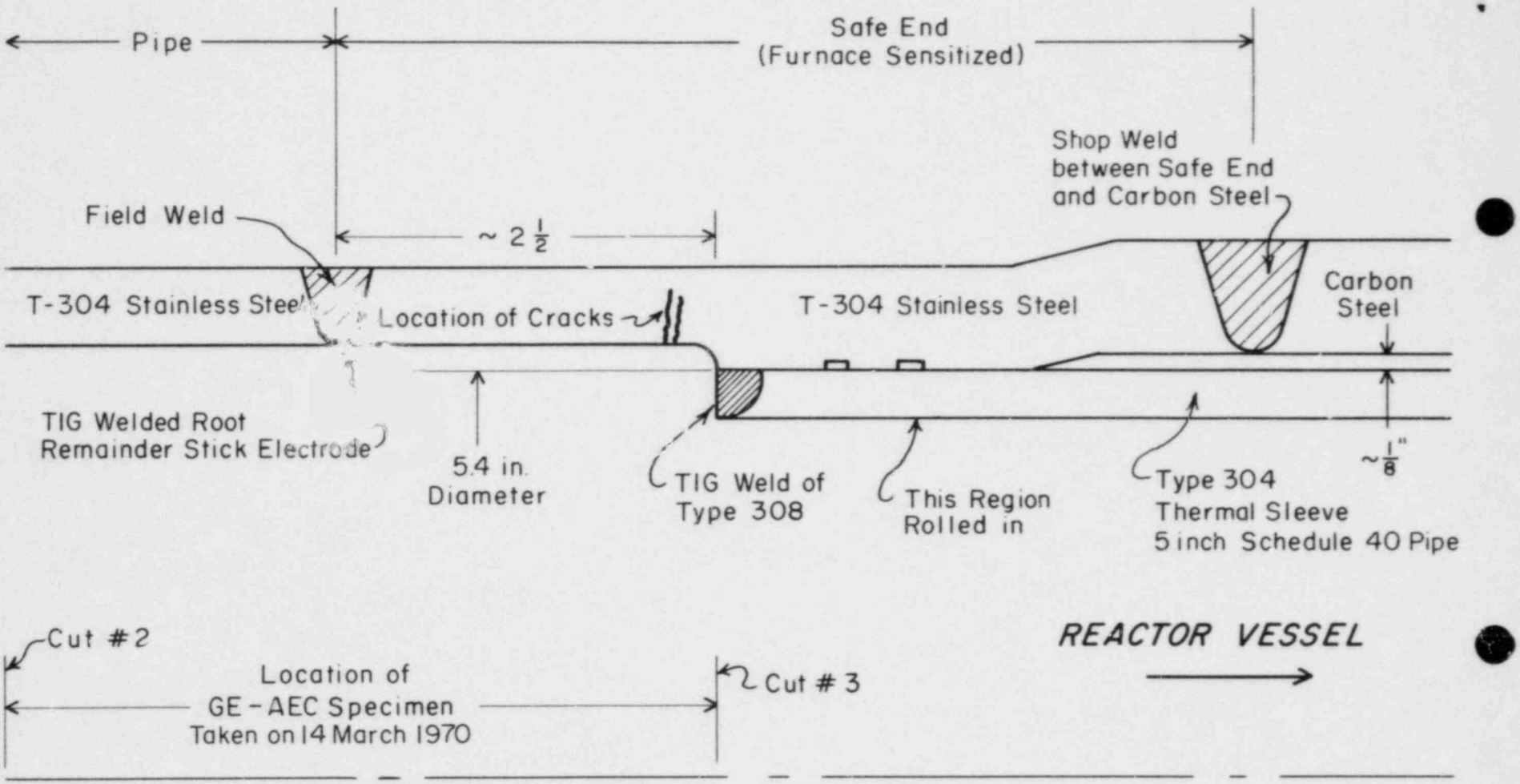

Figure 1. Schematic diagram showing safe end configuration.

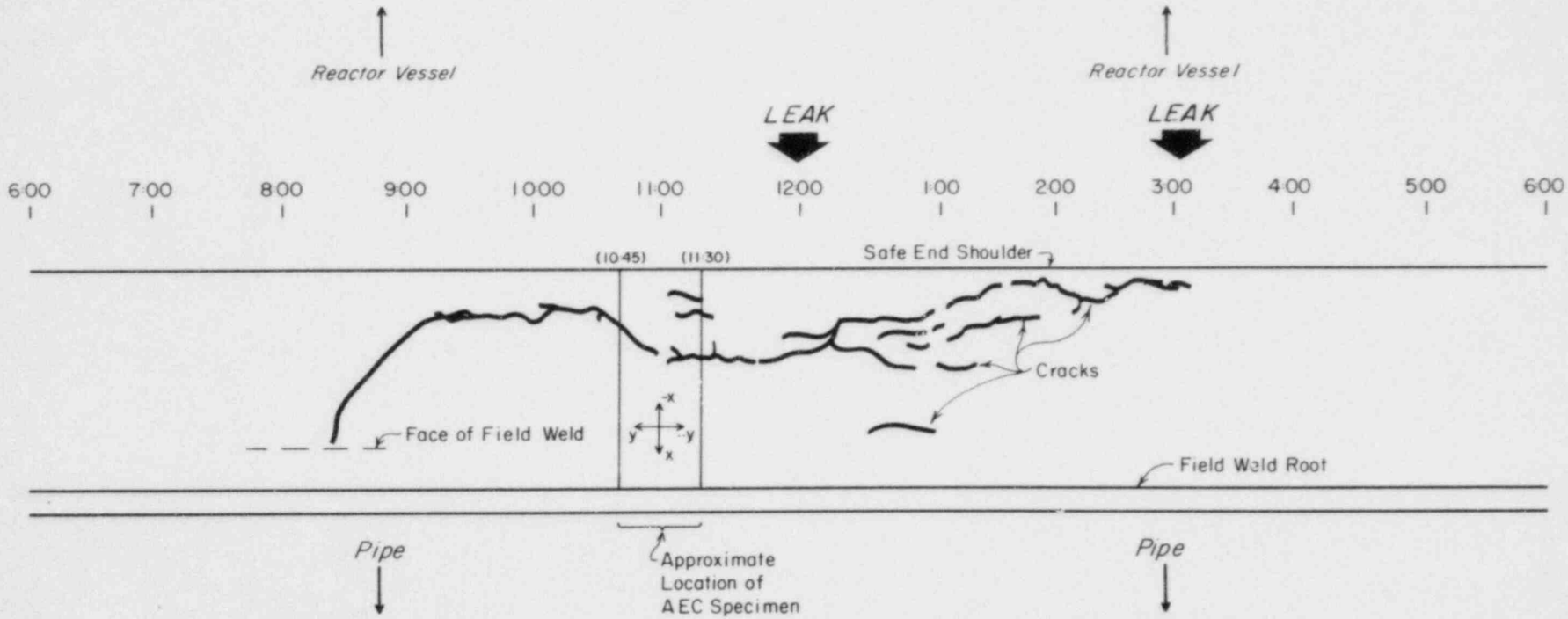

Figure 2. Schematic description of radiographic indications from safe end showing location of cracks. The 12:00 position was the top of the tube. Radiographs were taken through the double thickness of the tube before specimens were removed. Location of the AEC specimen is noted. Approximate location of leaks noted.

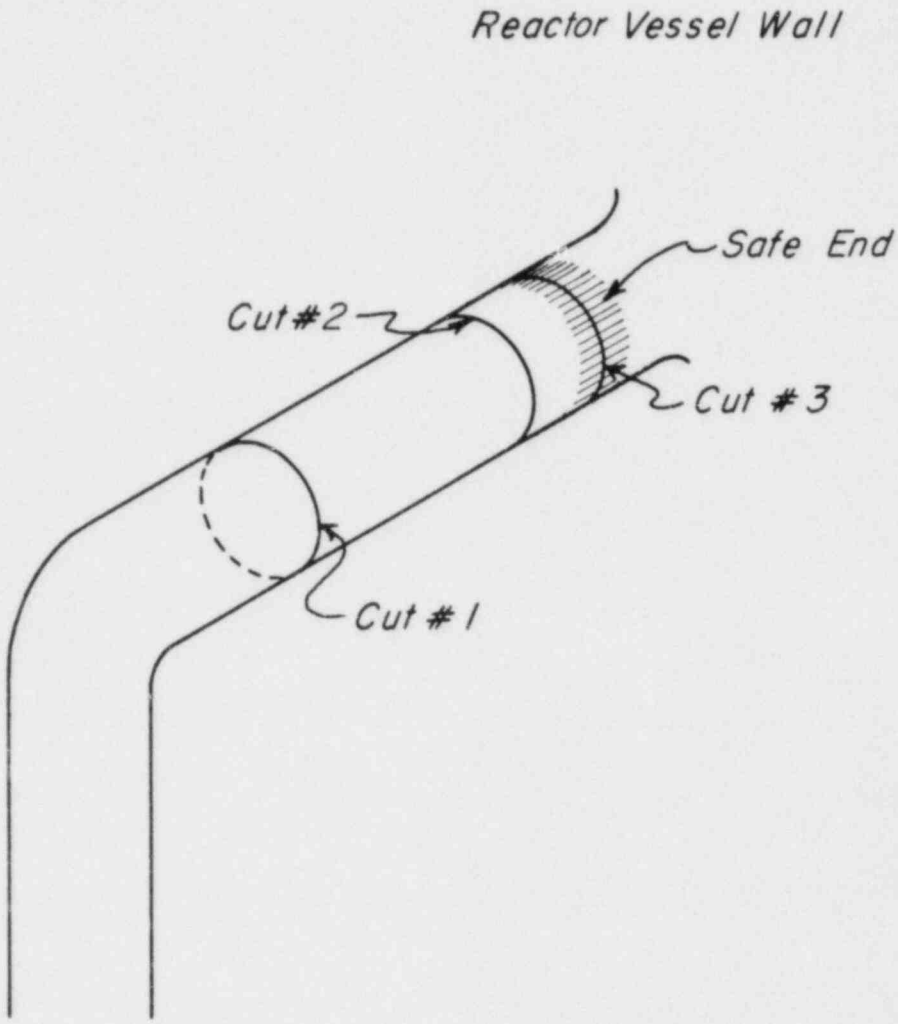

Figure 3. Schematic location of cuts made in the core spray line for removing the AEC-GE specimen. Cut numbers refer to same numbers of figure 1.

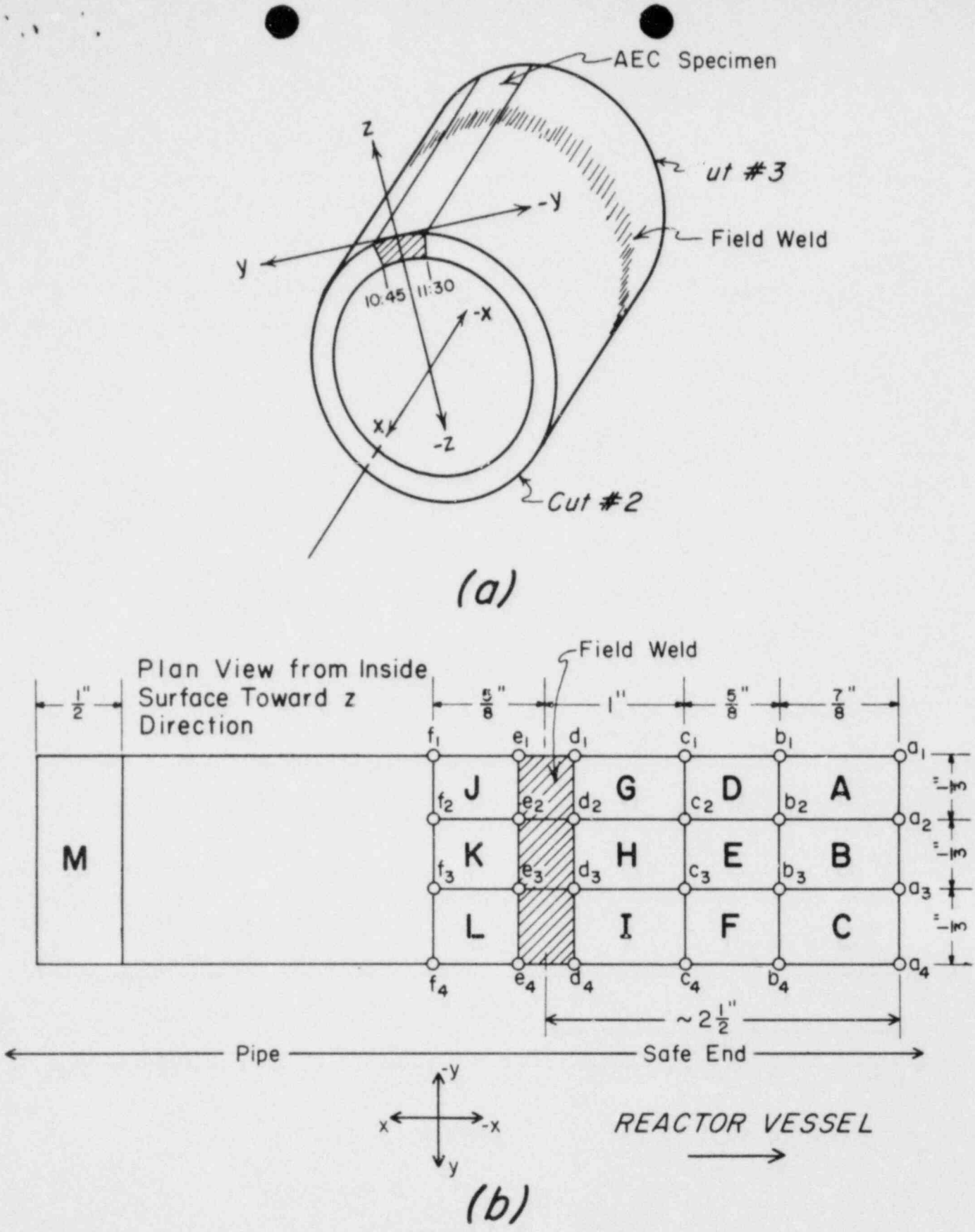

Figure 4. Schematic arrangement showing orientation and description of AEC specimen. (a) Orientation of specimen with respect to tube and coordinate axes. (b) Letter designations describing specimens taken from AEC specimen, together with coordinate axes.

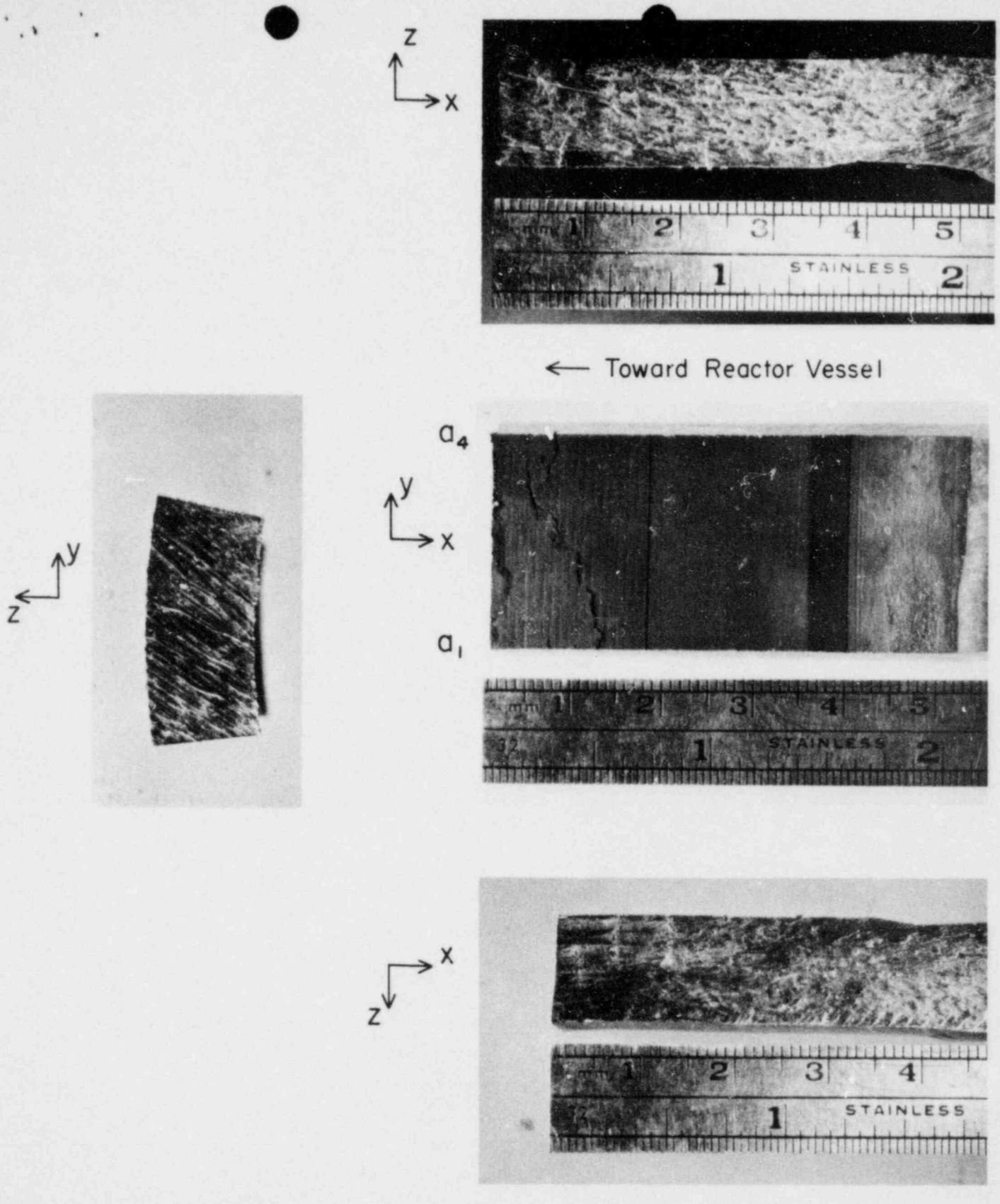

(c)

Figure 4. (c) Optical macrographs showing views of inside surface, edges, and end of AEC specimen. Only that portion shown in the -X direction from the field weld.

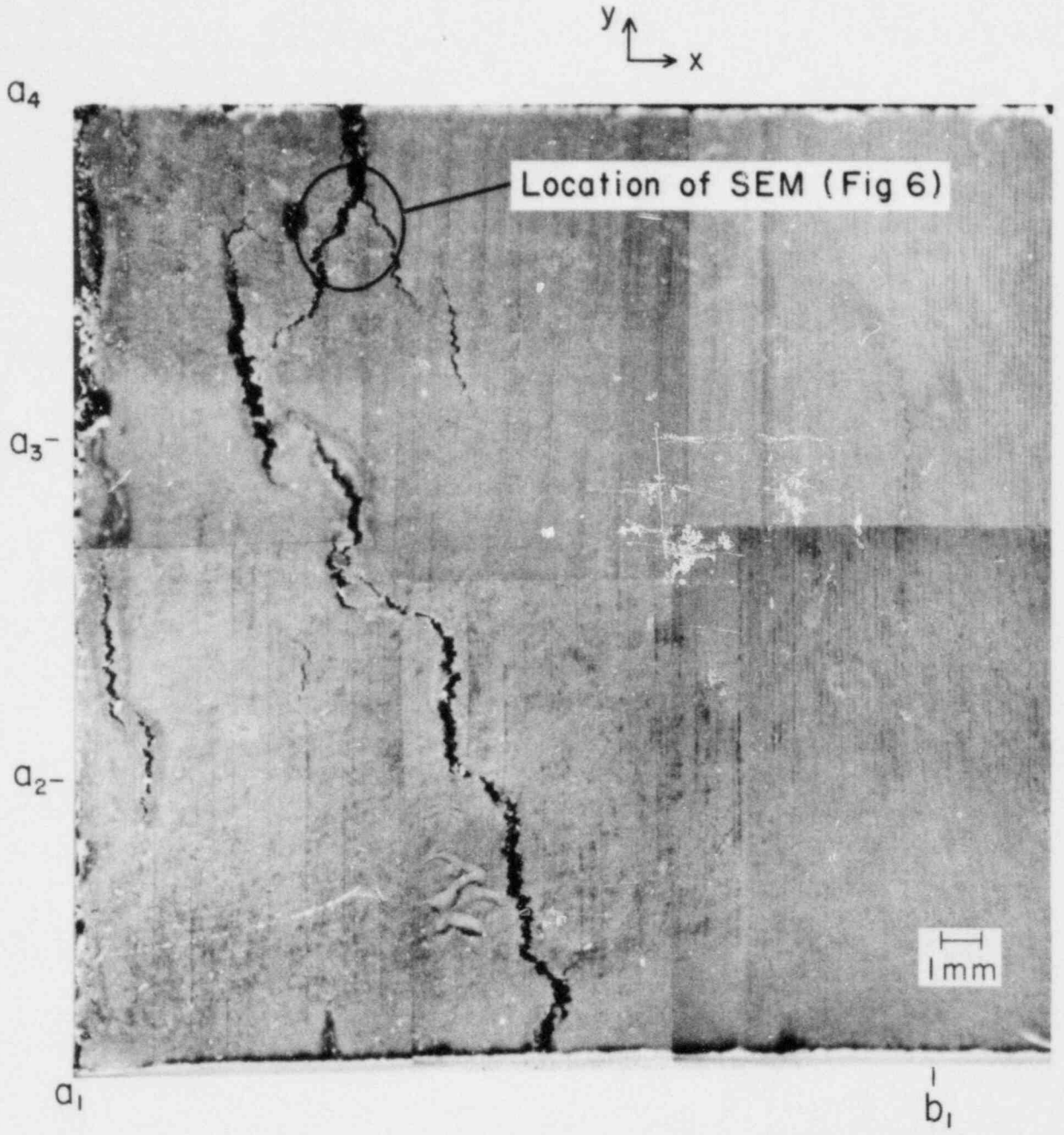

Figure 5. Optical macrograph showing view of inside surface of the AEC specimen. Coordinates relate to figure 4. Circled region shows site where scanning electron micrograph obtained (figure 6).

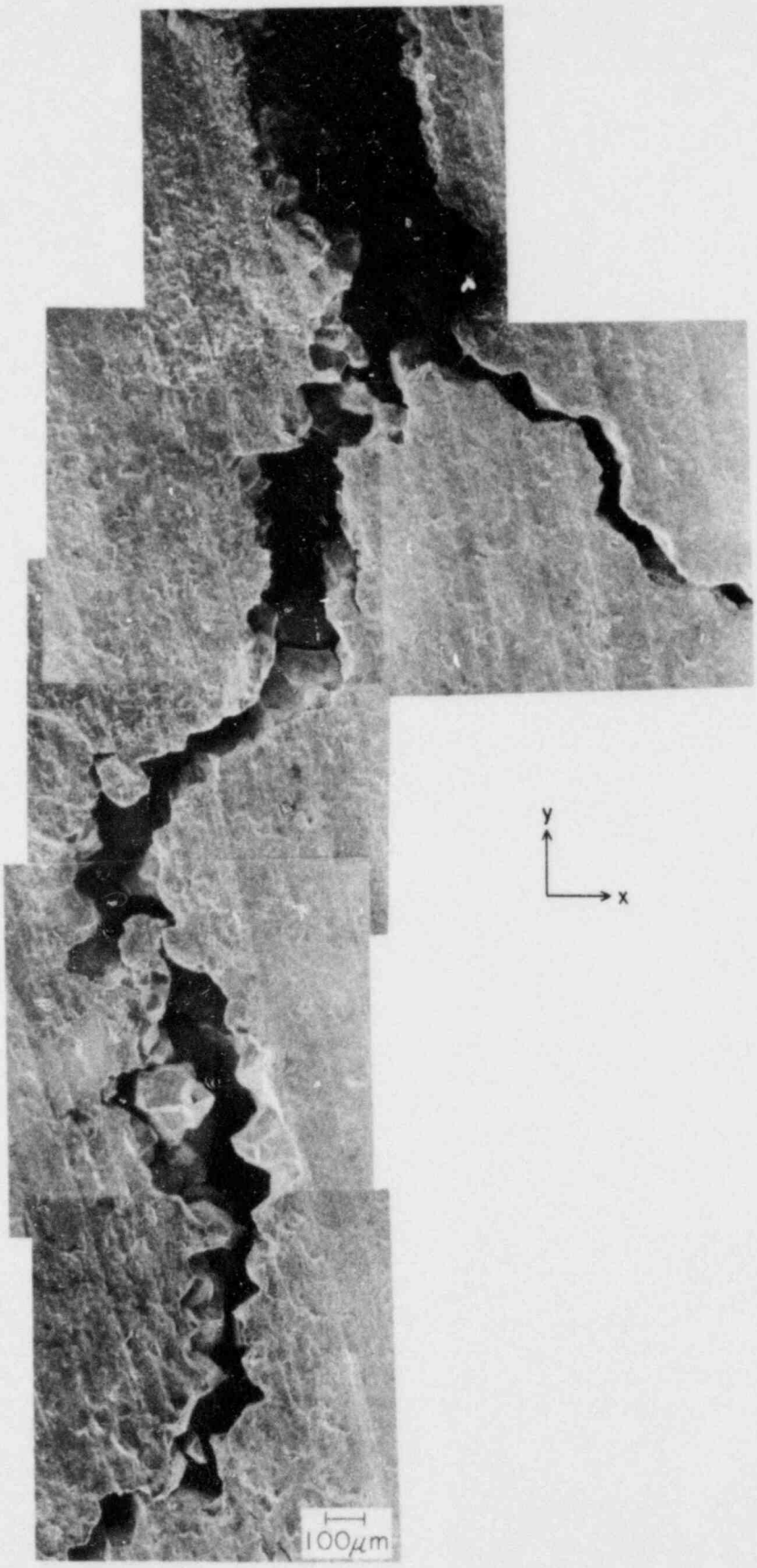

Figure 6. Scanning electron micrograph from inside surface of AEC specimen. Note site of micrograph in figure 5.

Figure 7. Optical micrograph of crack starting at inside surface and extending in the +z direction. Specimen taken from specimen B. Face being examined is in the x-z plane. Left figure is initial portion of crack and right figure is bottom. The bottom of the left figure and top of right are exactly contiguous.

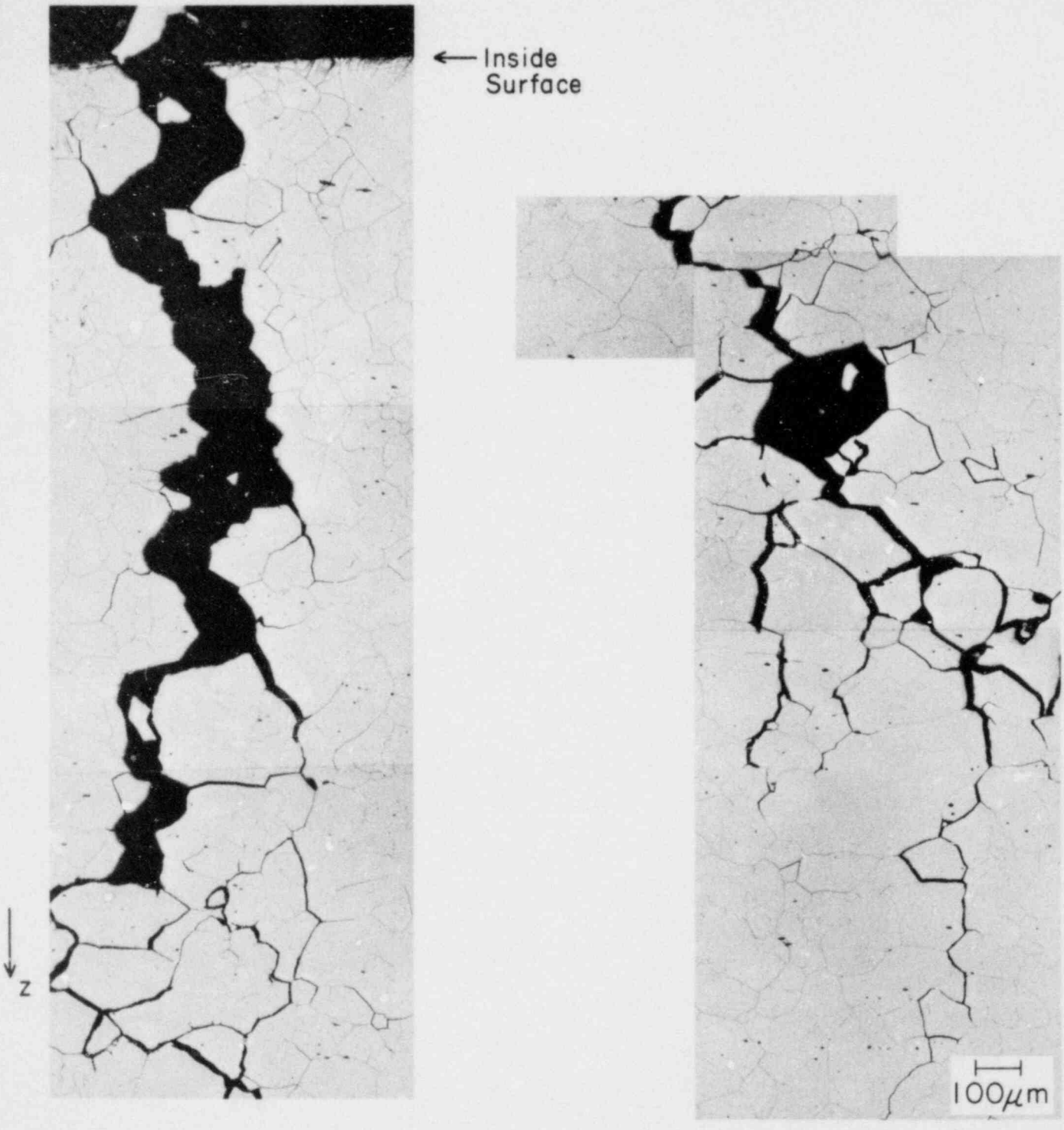

Figure 8. Optical micrograph of crack starting at inside surface and extending in the +z direction . Specimen taken from specimen B. Face being examined is in the x-z plane. Left figure is initial portion of crack and right figure is bottom. The bottom of the left figure and top of right are exactly contiguous.

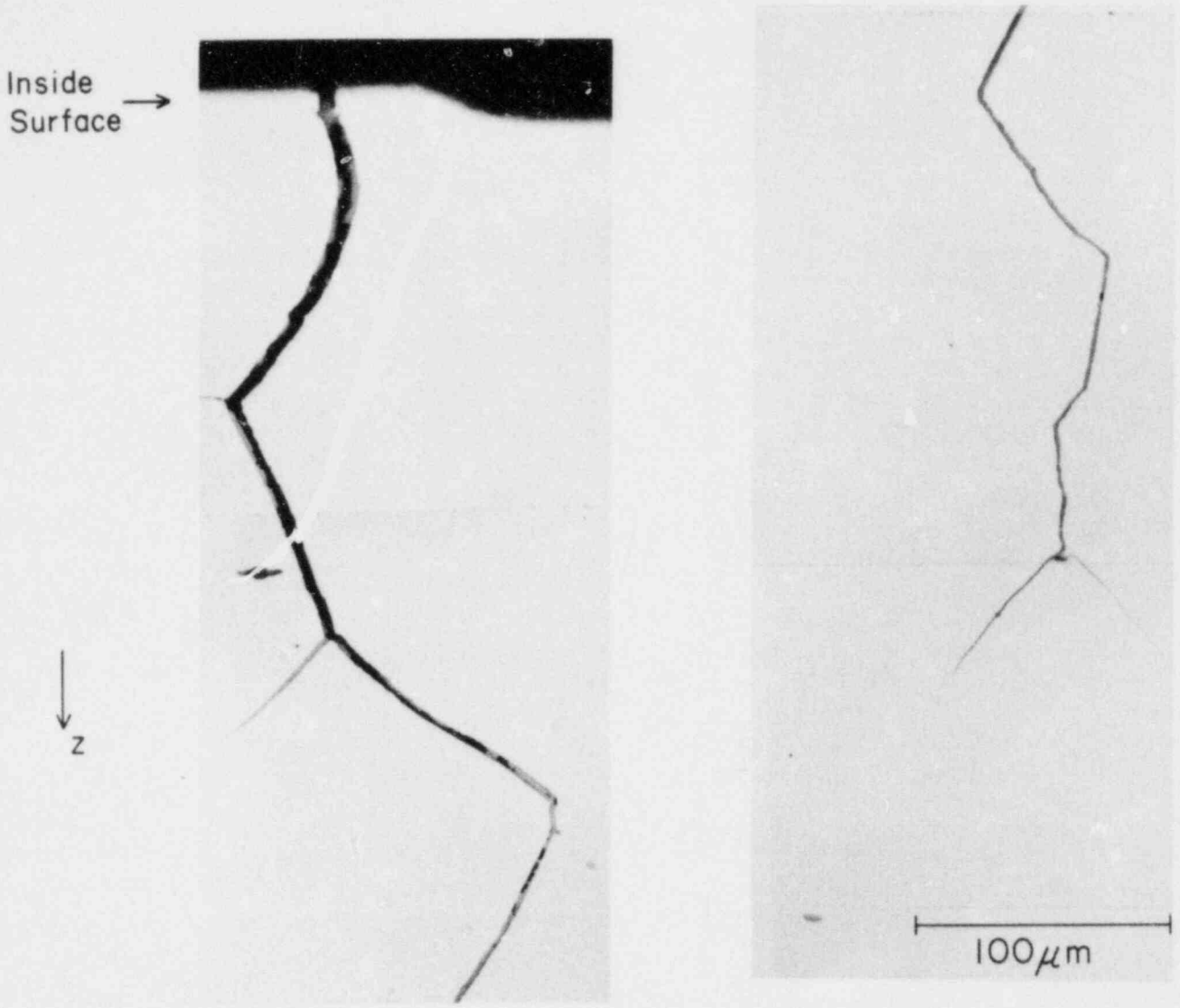

Figure 9. Optical micrograph of crack starting at inside surface and extending in the +z direction. Specimen taken from specimen E. Face being examined is in the x-z plane. Left figure is initial portion of crack and right figure is bottom. The bottom of the left figure and top of right are exactly contiguous.

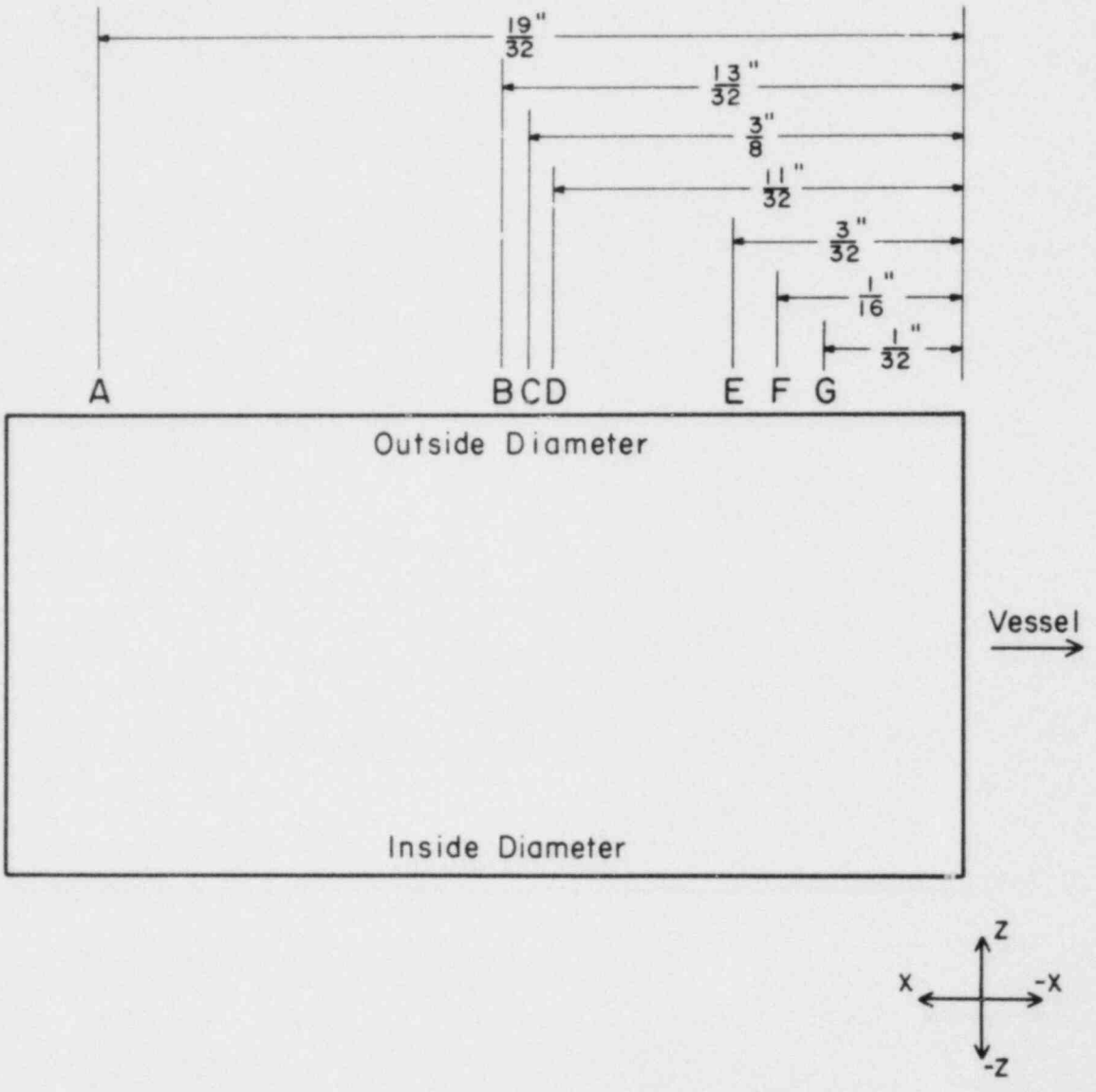

Figure 10. Schematic arrangement showing location of specimens taken from outside surface of specimen B. Surface viewed is in the x-z plane.

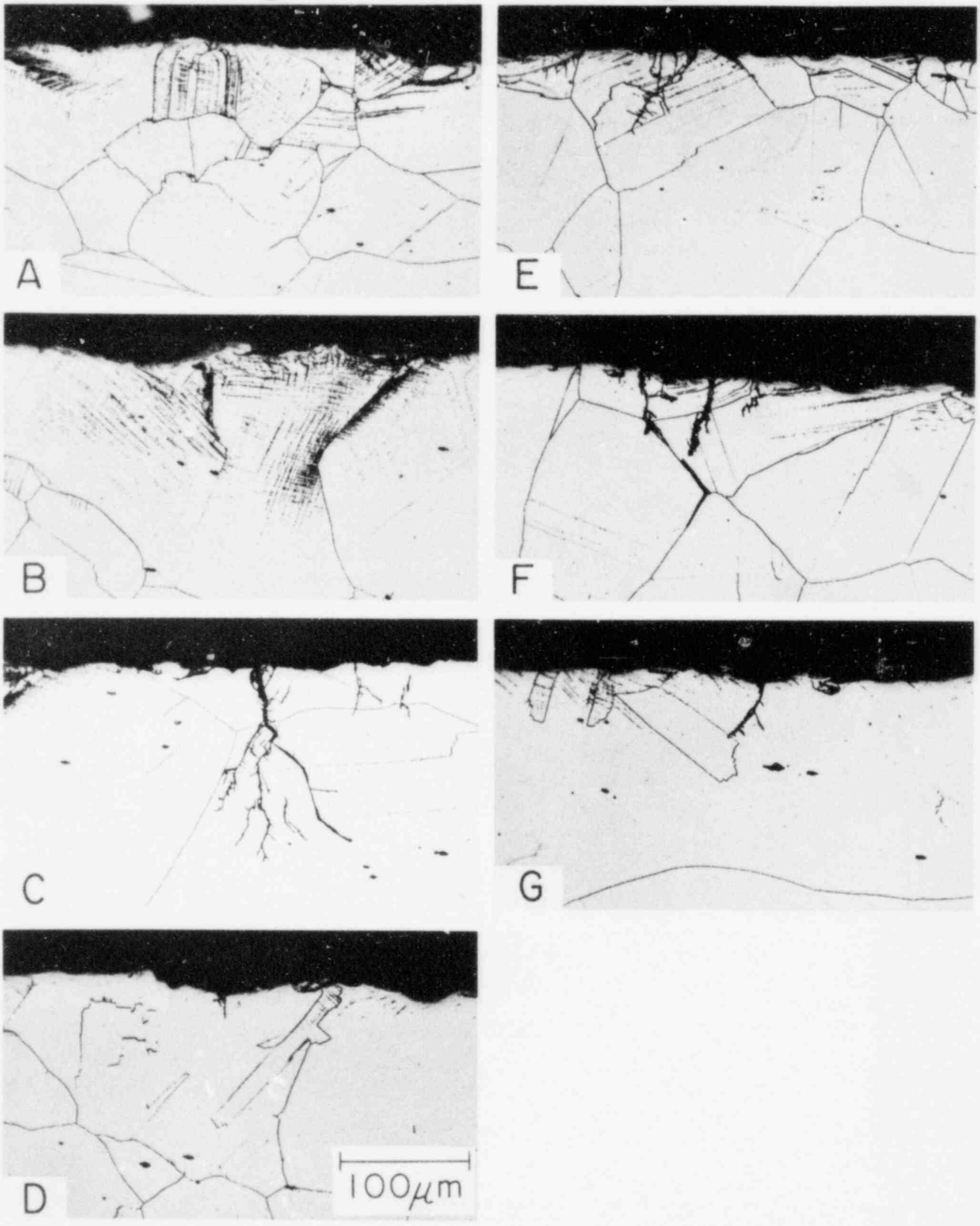

Figure 11. Photomicrographs of cracks on outside surface of specimen B. Cracks are propagating in the -z direction. Surface viewed is the x-z plane.

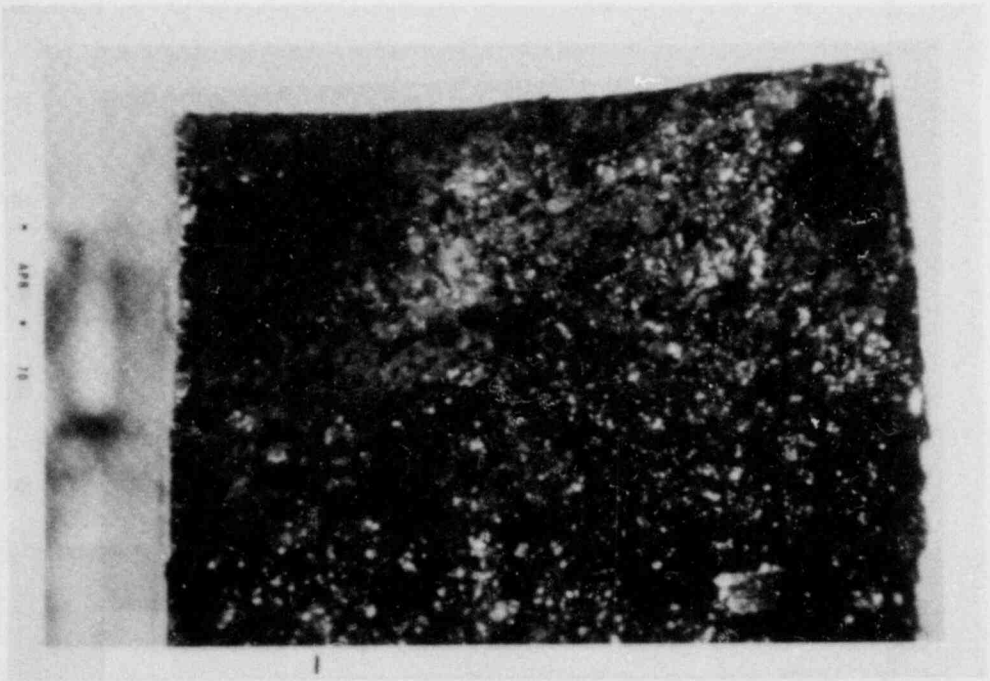

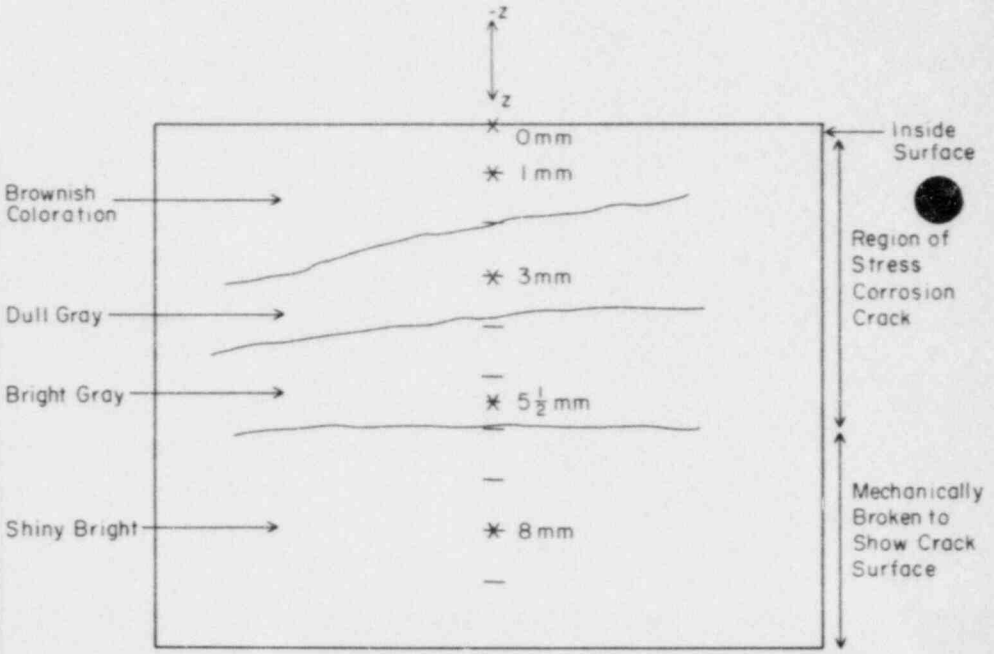

(a) (b)

Figure 12. View of face of crack. Crack face is in the y-z plane. Specimen broken apart for viewing. (a) Ektachrome color print and (b) Schematic diagram showing various regions of crack. Distances from inside surfaces noted locate sites where scanning micrographs taken. Specimen broken open to show surface of stress corrosion crack. Shiny bright region results from this breaking process.

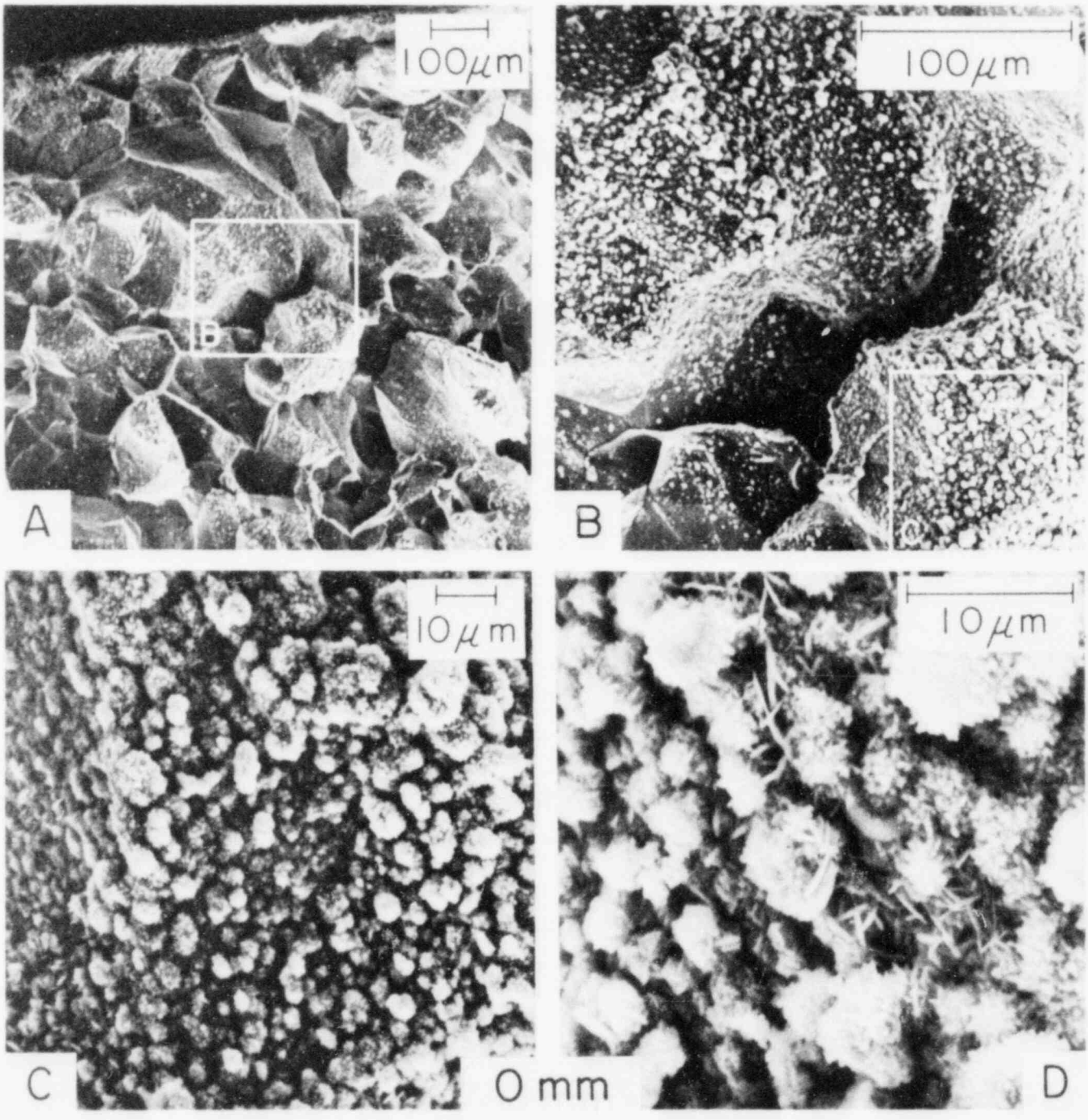

Figure 13. Scanning electron micrographs of stress corrosion crack surface corresponding to 0 mm position noted in figure 12.

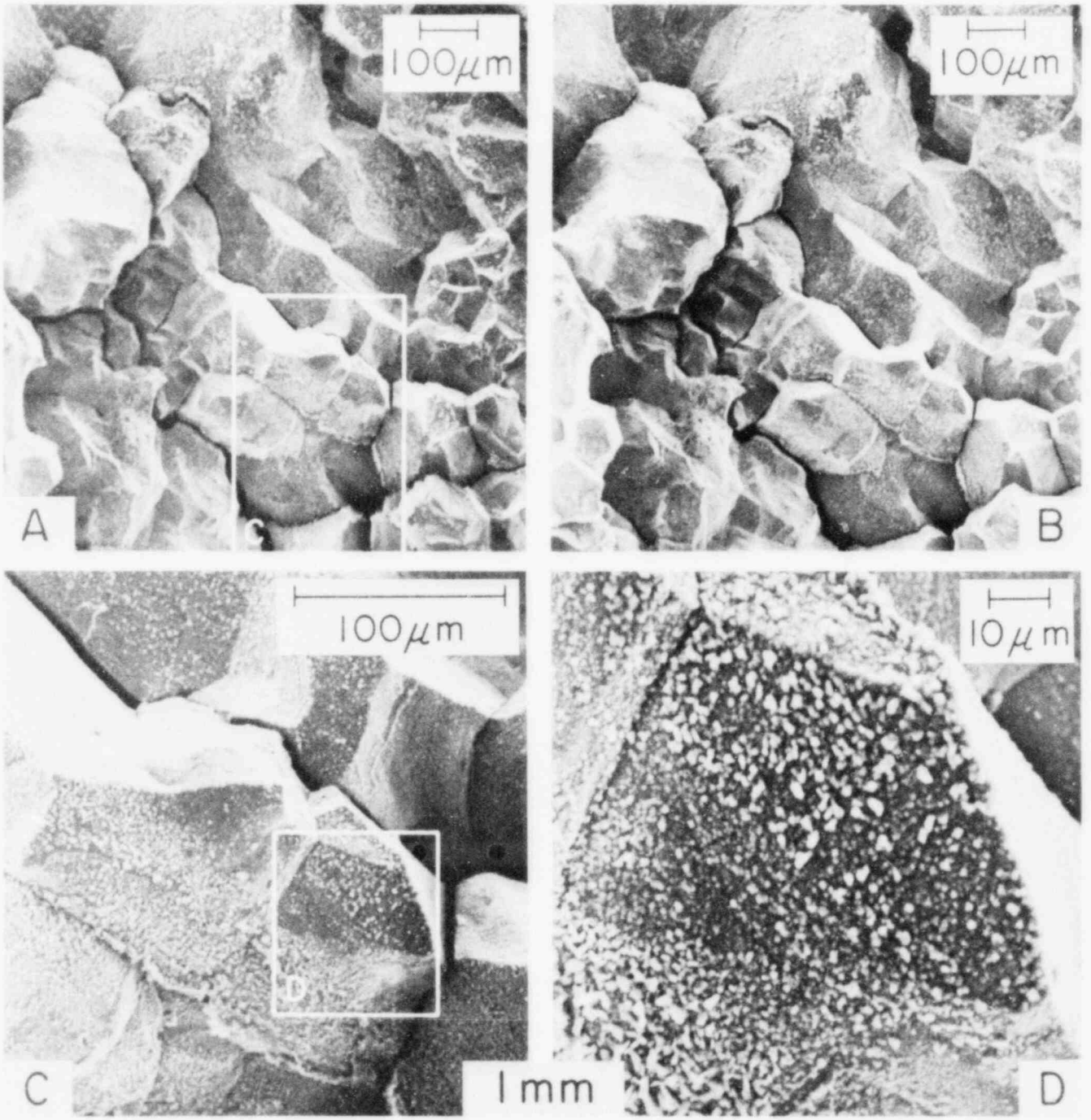

Figure 14. Scanning electron micrographs of stress corrosion crack surface corresponding to 1 mm position noted in figure 12.

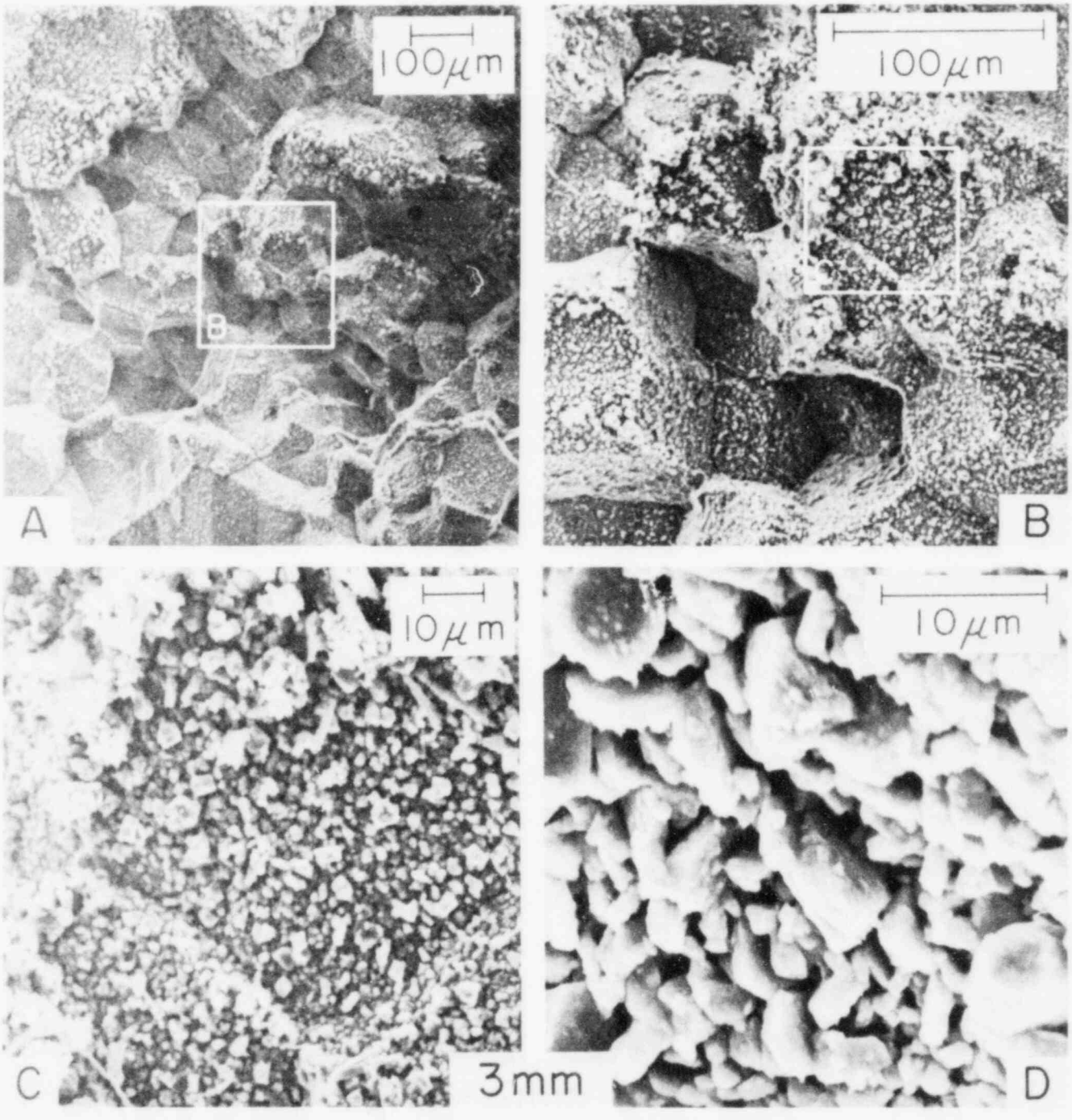

Figure 15. Scanning electron micrographs of stress corrosion crack surface corresponding to 3 mm position noted in figure 12.

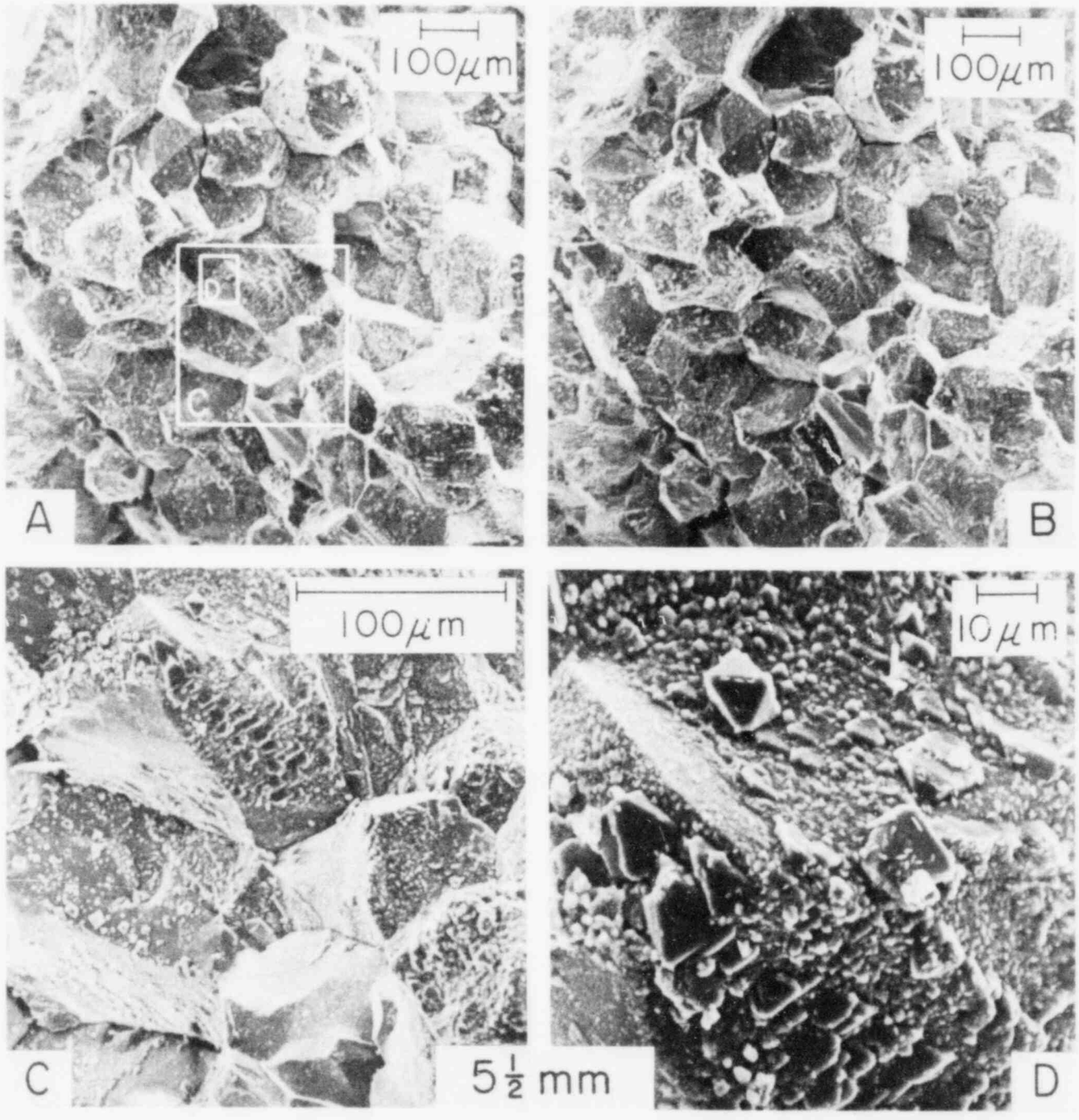

Figure 16. Scanning electron micrographs of stress corrosion crack surface corresponding to 5-1/2 mm position noted in figure 12.

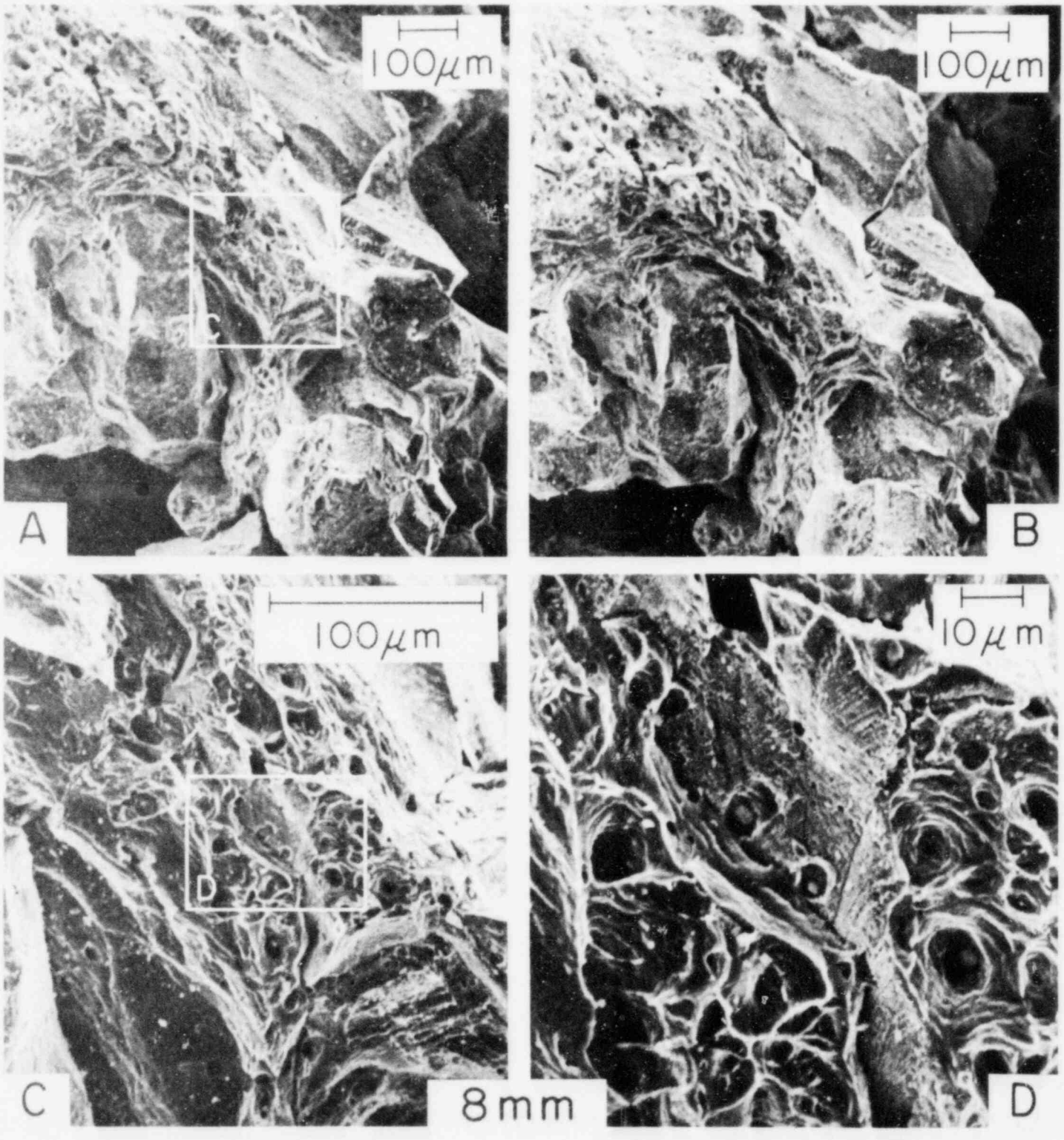

Figure 17. Scanning electron micrographs of stress corrosion crack surface corresponding to 8 mm position noted in figure 12.

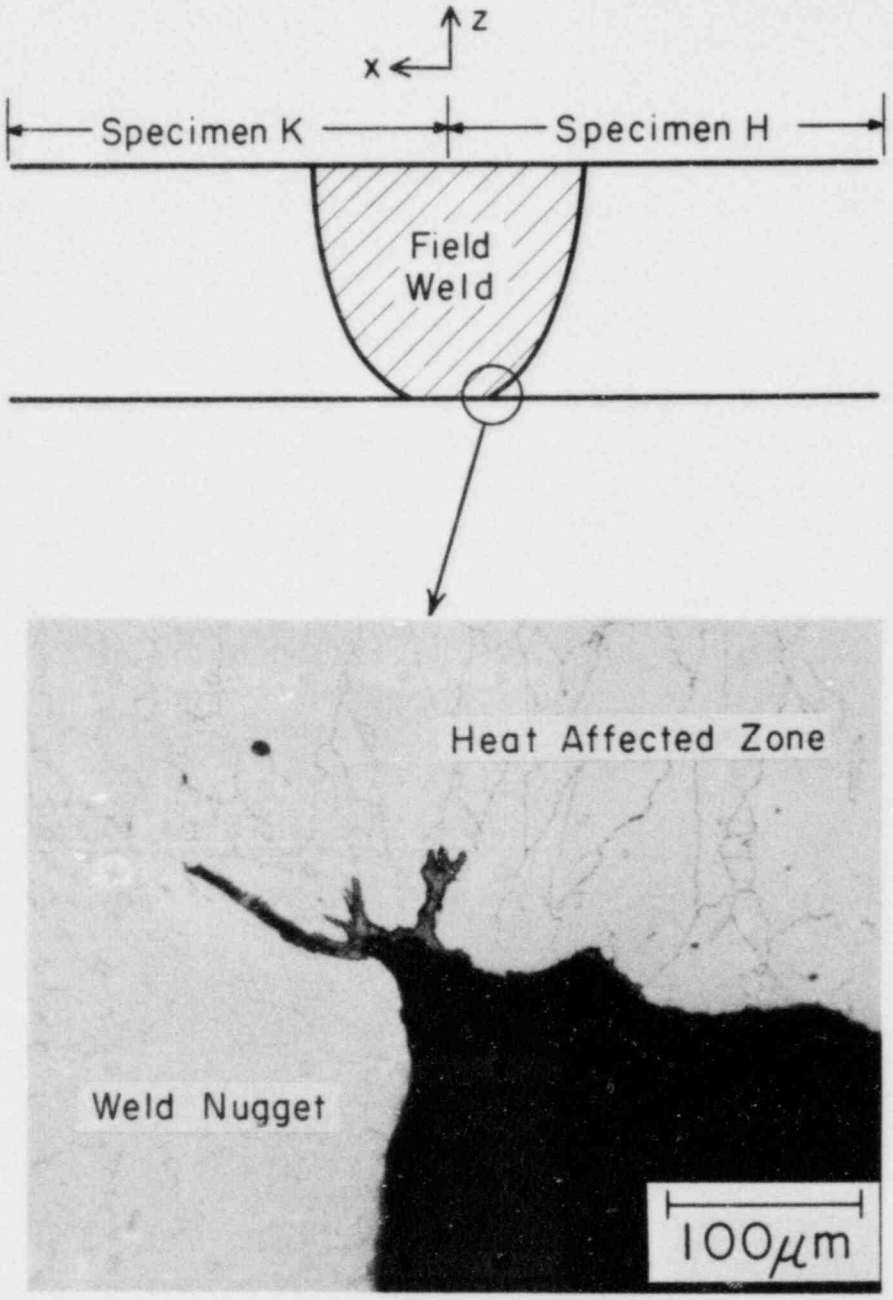

Figure 18. Optical micrograph from specimen H along inside surface along d_2-d_3. Plane viewed is x-z.

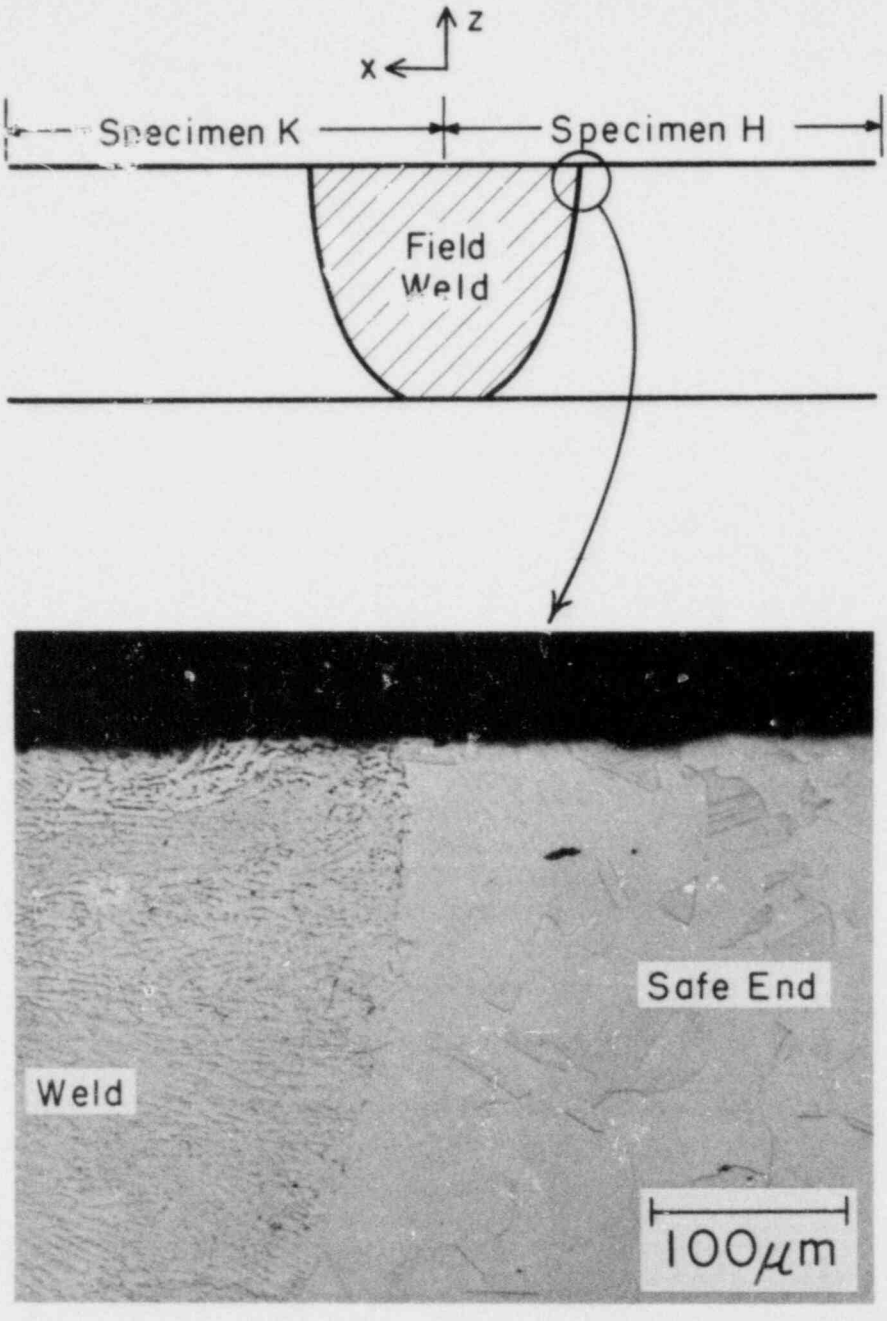

Figure 19. Optical micrograph from specimen H along the outside surface along d_2-d_3. Plane viewed is x-z.

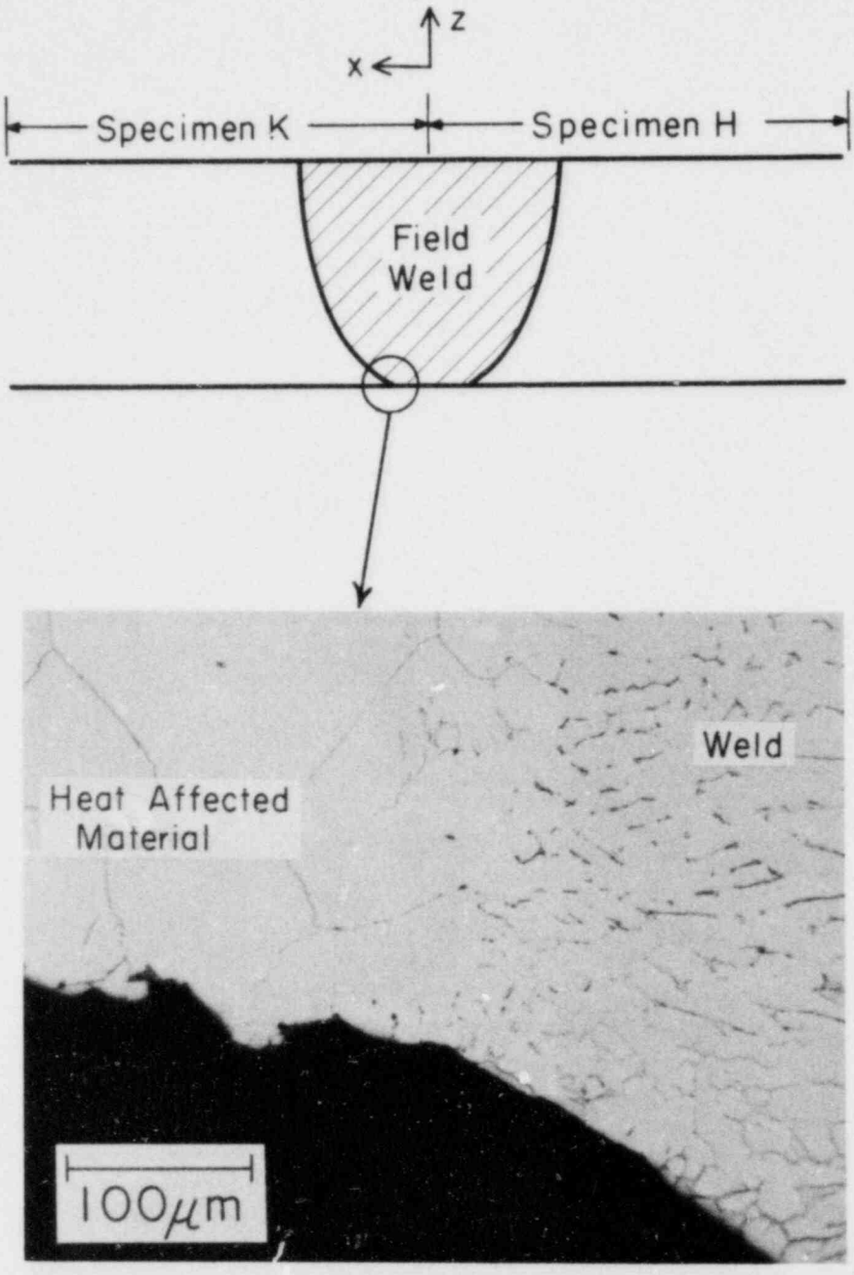

Figure 20. Optical micrograph from specimen K showing inside surface along e_2-e_3. Plane viewed is x-z.

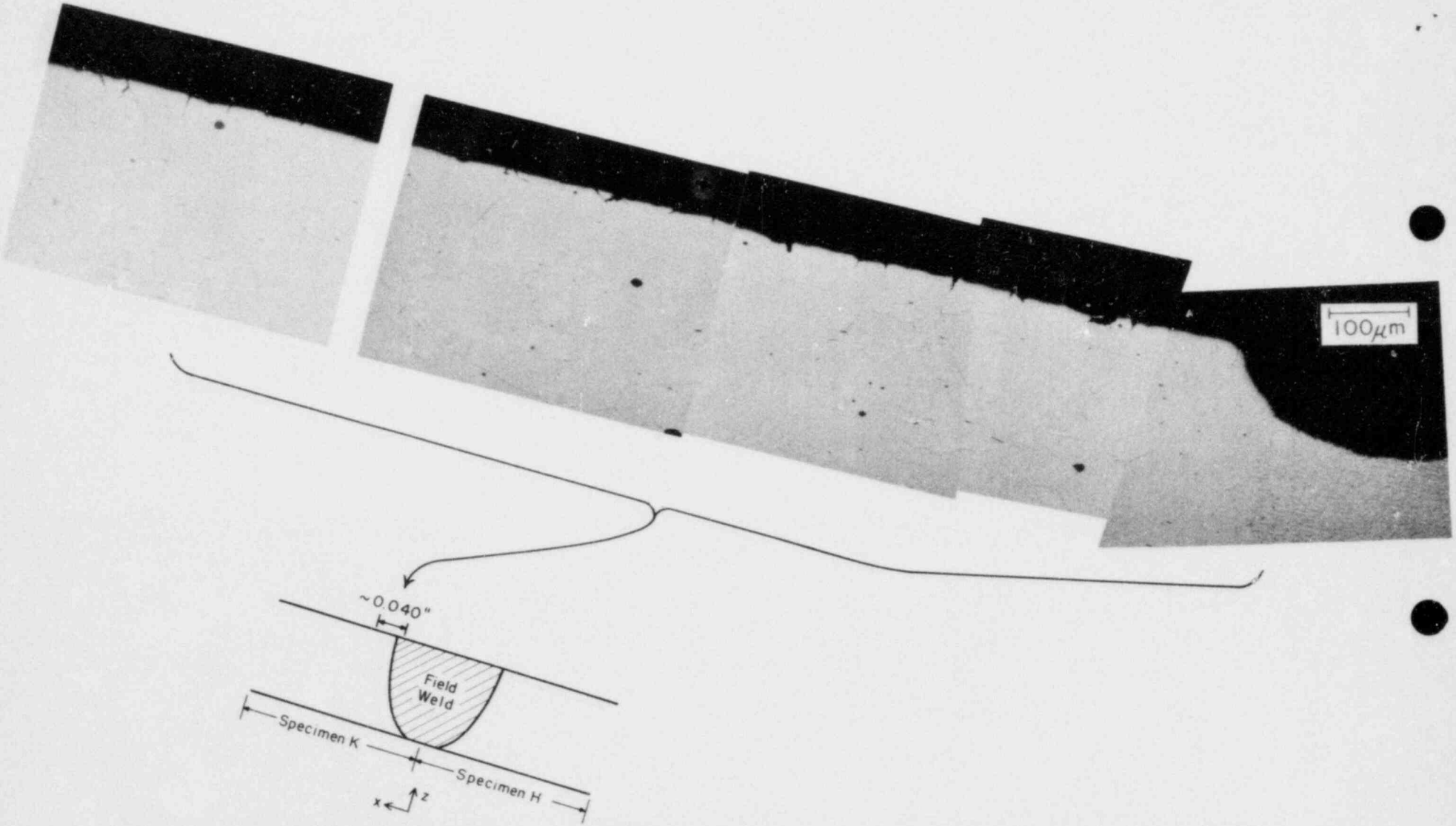

Figure 21. Optical micrographs from specimen K showing outside surface. Penetrations are extending in the -z direction from the surface. The plane viewed here is along the e_2-f_2 line.

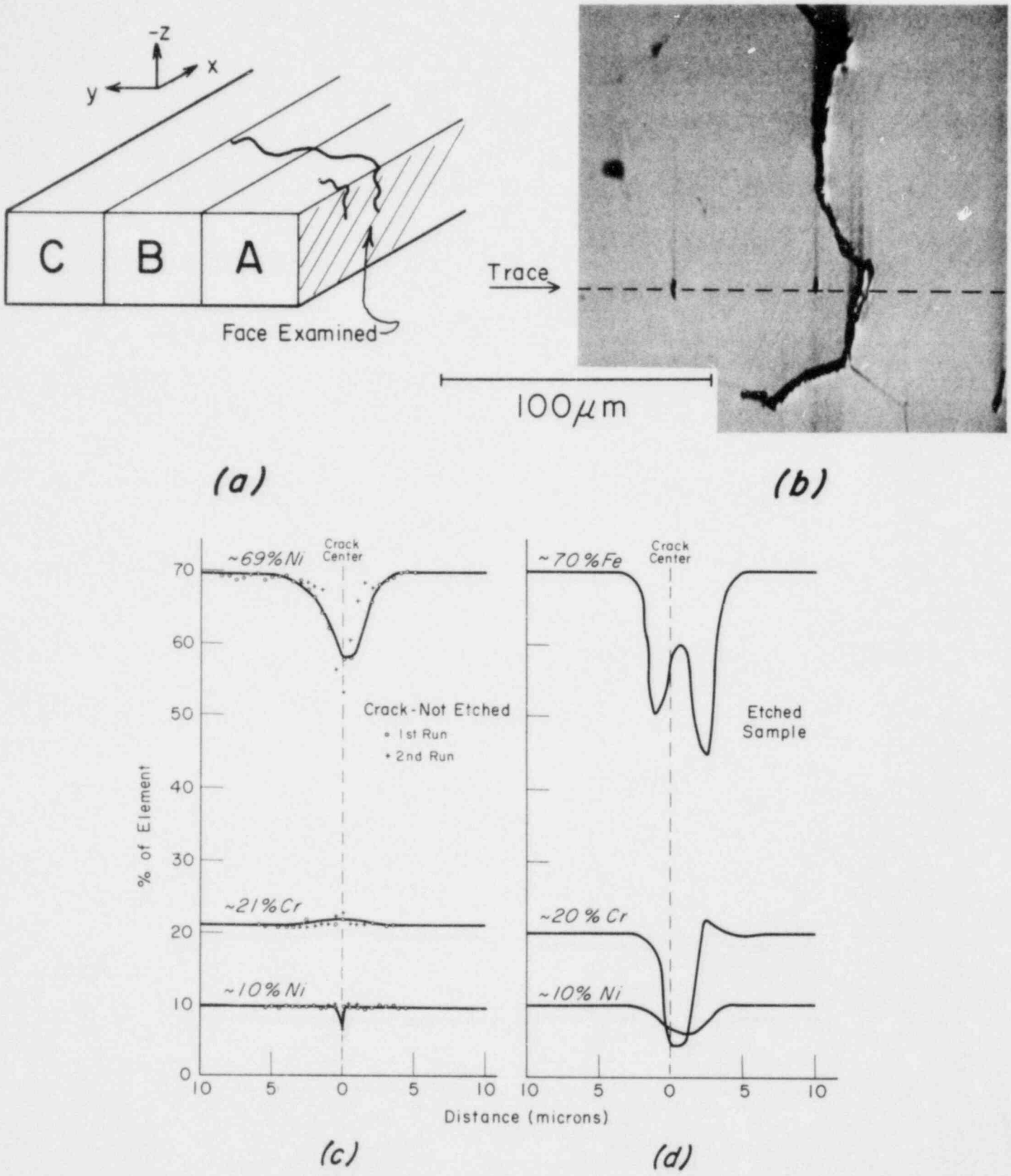

Figure 22. (a) Schematic location showing where microprobe trace across crack was performed. (b) Photographs showing where traces performed. (c) - (d) Results from separate determination at different sites along crack.

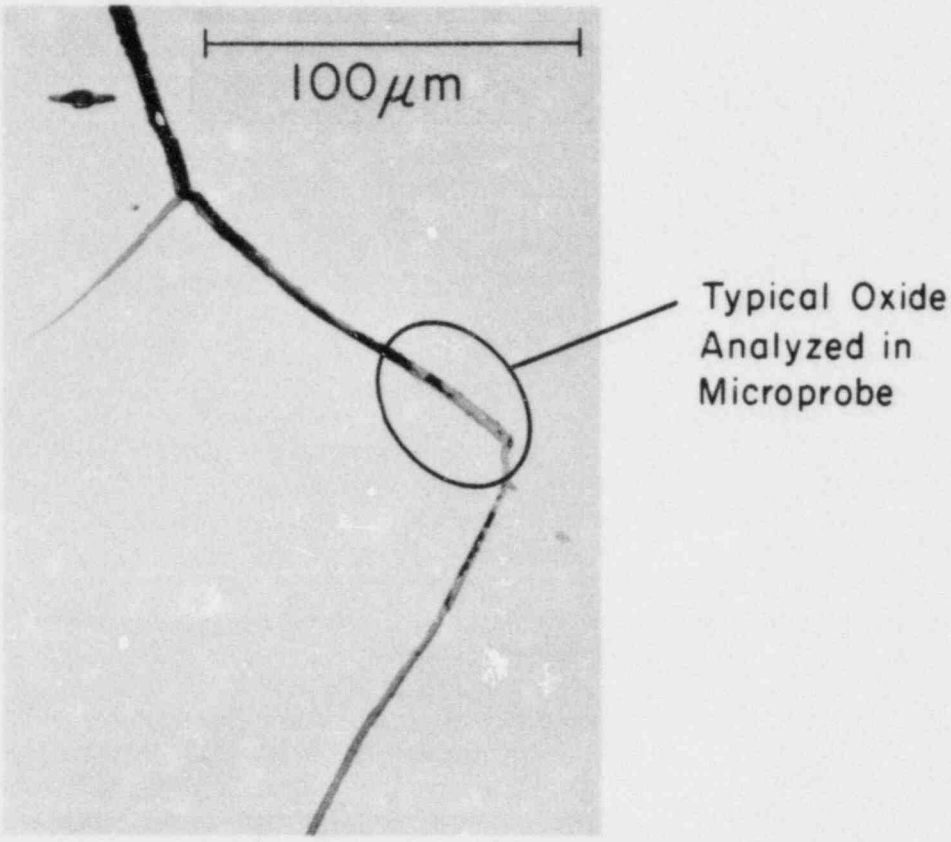

Figure 23. Typical oxide in crack showing where the x-ray spectrum was analyzed. This is not the region examined but the oxide is typical.

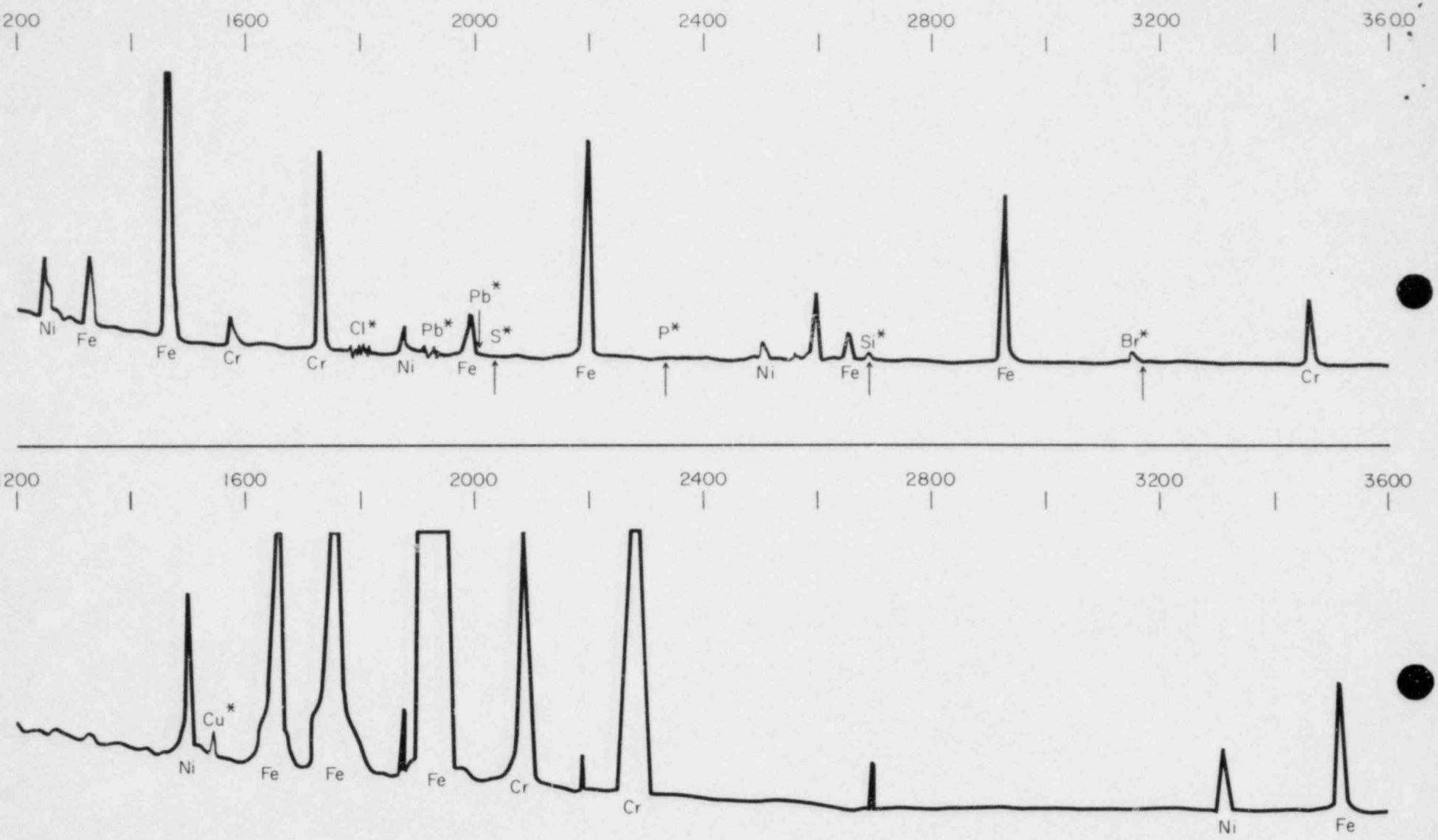

Figure 24. Intensity of x-ray emissions from spectral scan of one piece of oxide in crack by microprobe. Special regions where primary peaks should have occurred for particularly sought elements as noted with asterisk.

Figure 25. Montage showing scanning micrograph from face of stress corrosion crack. Special notations locate regions where microprobe determination were made. The location of each micrograph is the same as that in figure 12. Most of the scanning micrographs are from the series shown in figures 13-17. For reference the Cr/Fe ratio of scale-free type 304 stainless steel is 0.4. These ratios are from direct scale readings and are not corrected.

Scanning Electron Micrograph

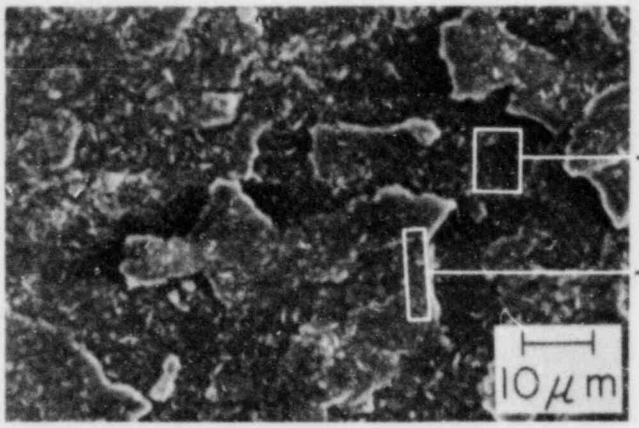

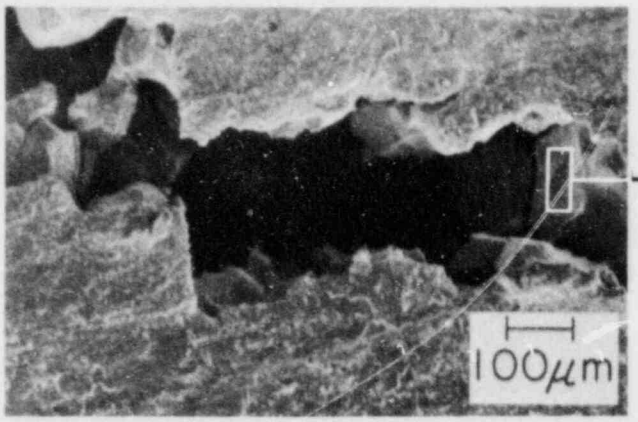

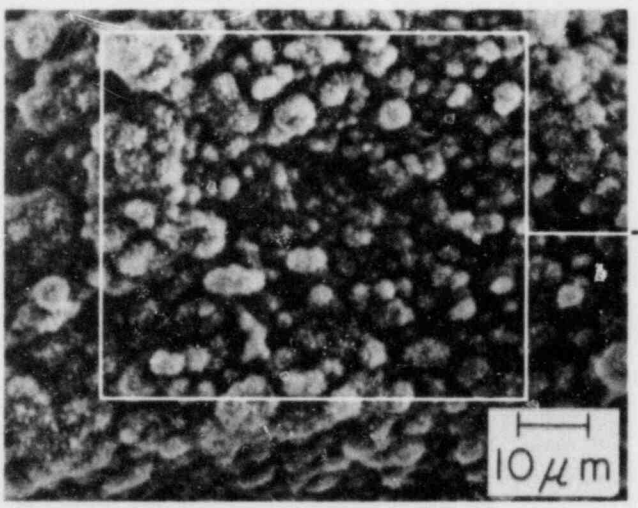

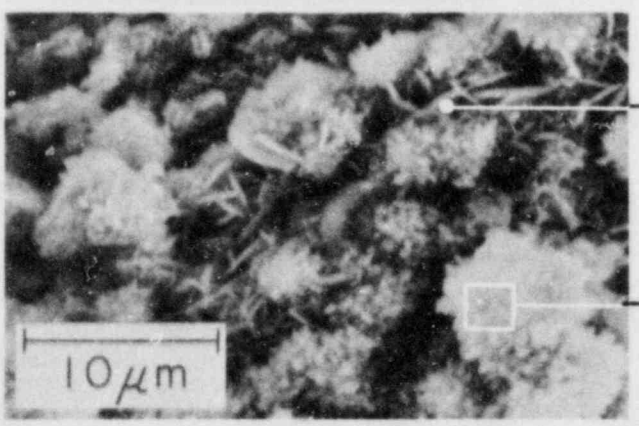

POSITION	Cr/Fe RATIO
A	A = 4.0 (surface scale flake)
B - Inside Surface (x-y plane)	B = 3.0 (surface scale)
C - Broken Grain Near Crack Mouth	C = 1.7
D 0 mm Lower Magnification	D = 25
E 0 mm Higher Magnification	E = 19 "Pebbles"
F	F = 5.6 "Needles"

Scanning Electron Micrograph

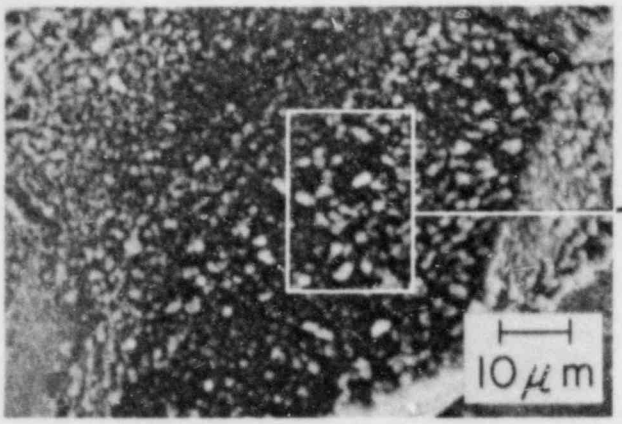

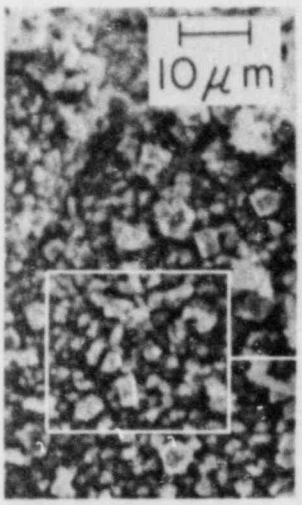

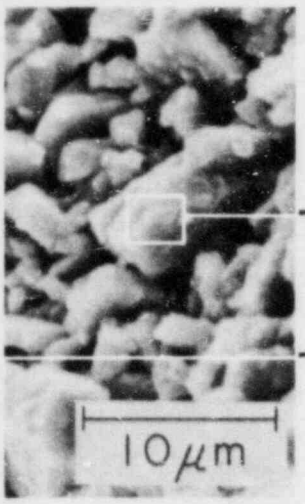

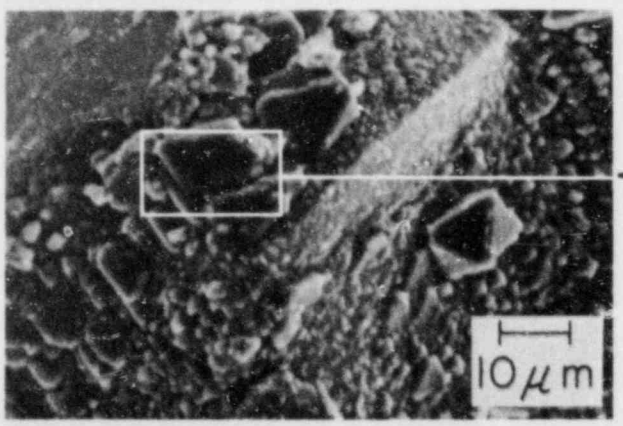

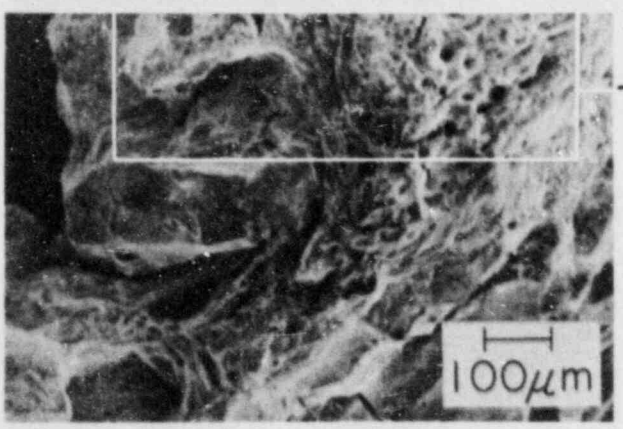

POSITION	Cr/Fe RATIO
G 1 mm	G = 0.7
I 3 mm	I = 0.025 (higher magnification)
H	H = 0.8 (lower magnification)
J 5 1/2 mm	J = 1.4
K 8 mm	K = 0.5

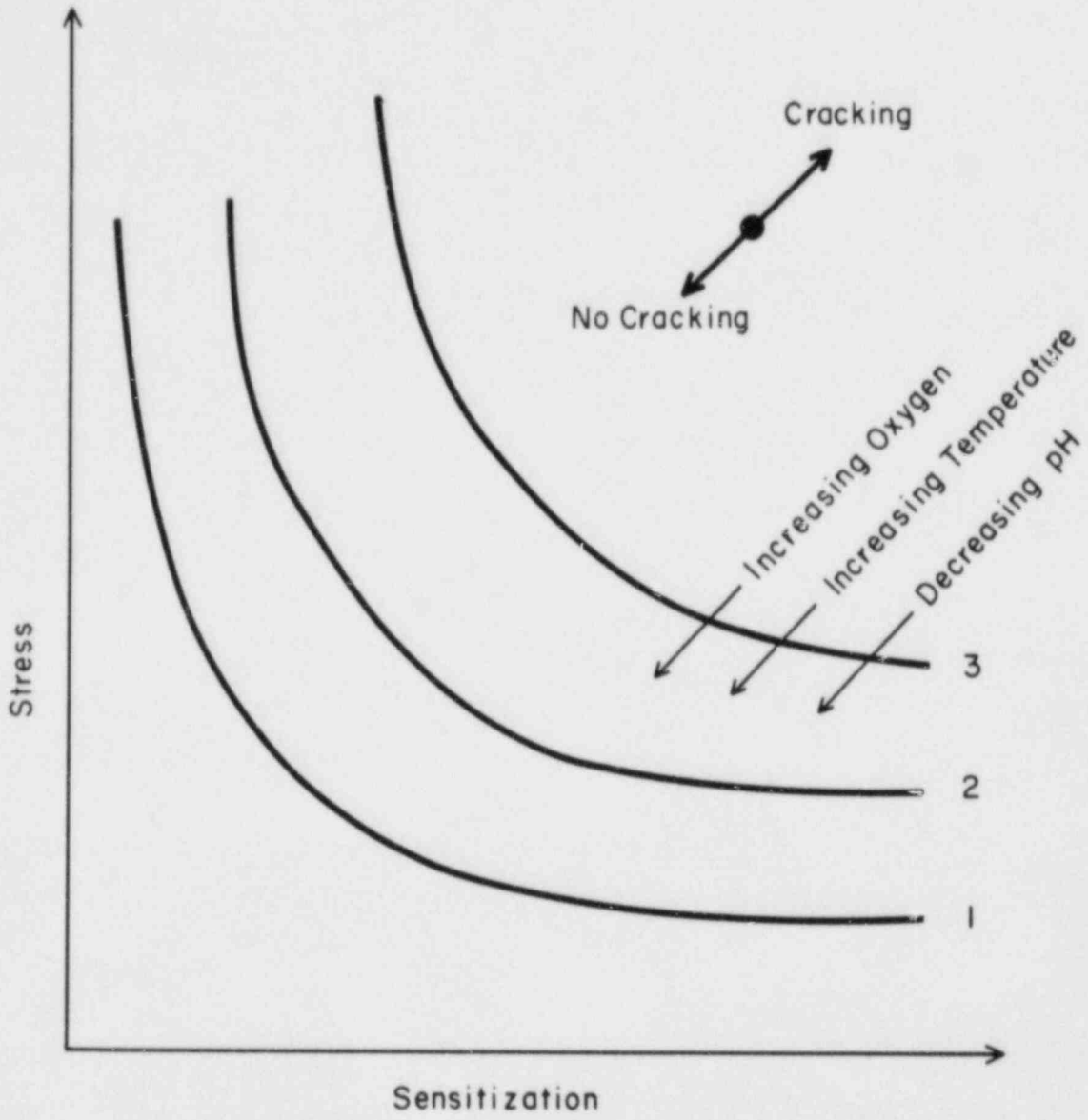

Figure 26. Schematic relationship showing possible pattern of interaction of stress, sensitization, dissolved oxygen, temperature and pH in the stress corrosion cracking of sensitized stainless steels.